Cell

PNMA2 forms immunogenic non-enveloped virus-like capsids associated with paraneoplastic neurological syndrome

Graphical abstract

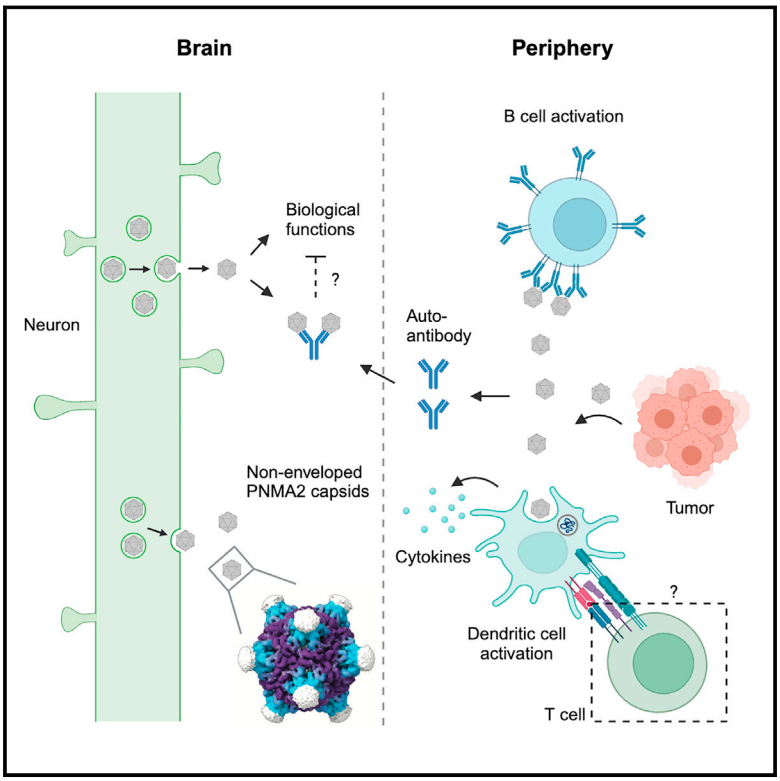

Highlights

- Gag-derived PNMA2 protein is released from cells as non-enveloped virus-like capsids
- Recombinant PNMA2 capsids injected into mice induce an autoimmune reaction
- Mouse and paraneoplastic patient PNMA2 autoantibodies bind to external capsid epitopes
- Mice injected with PNMA2 capsids develop learning and memory deficits

Authors

Junjie Xu, Simon Erlendsson, Manvendra Singh, ..., Cédric Feschotte, John A.G. Briggs, Jason D. Shepherd

Correspondence

jason.shepherd@neuro.utah.edu

In brief

PNMA2 is a domesticated retrotransposon gene associated with cancer-induced paraneoplastic neurological syndromes. Findings here show that PNMA2 protein is exclusively expressed in the brain of mammals and is released as non-enveloped virus-like capsids, which are immunogenic and induce an autoimmune response that leads to neurological deficits when injected into mice.

Xu et al., 2024, Cell *187*, 831–845
February 15, 2024
https://doi.org/10.1016/j.cell.2024.01.009

CellPress

Cell

CellPress

Article

PNMA2 forms immunogenic non-enveloped virus-like capsids associated with paraneoplastic neurological syndrome

Junjie Xu,[1] Simon Erlendsson,[2,3] Manvendra Singh,[4] G. Aaron Holling,[5] Matthew Regier,[1] Iosune Ibiricu,[6] Jenifer Einstein,[1] Michael P. Hantak,[1] Gregory S. Day,[7] Amanda L. Piquet,[8] Tammy L. Smith,[9] Stacey L. Clardy,[9] Alexandra M. Whiteley,[5] Cédric Feschotte,[4] John A.G. Briggs,[2,6] and Jason D. Shepherd[1,10,11,*]

[1]Department of Neurobiology, University of Utah, Salt Lake City, UT, USA
[2]The Medical Research Council Laboratory of Molecular Biology, Francis Crick Avenue, Cambridge, UK
[3]Novo Nordisk Foundation Center for Protein Research, University of Copenhagen, Copenhagen, Denmark
[4]Department of Molecular Biology and Genetics, Cornell University, Ithaca, NY, USA
[5]Department of Biochemistry, University of Colorado Boulder, Boulder, CO, USA
[6]Department of Cell and Virus Structure, Max Planck Institute of Biochemistry, Martinsried, Germany
[7]Department of Neurology, Mayo Clinic, Jacksonville, FL, USA
[8]Department of Neurology, University of Colorado, Aurora, CO, USA
[9]Department of Neurology, University of Utah and George E Wahlen VA Medical Center, Salt Lake City, UT, USA
[10]X (formerly Twitter): @jasonsynaptic
[11]Lead contact
*Correspondence: jason.shepherd@neuro.utah.edu
https://doi.org/10.1016/j.cell.2024.01.009

SUMMARY

The paraneoplastic Ma antigen (PNMA) proteins are associated with cancer-induced paraneoplastic syndromes that present with an autoimmune response and neurological symptoms. Why PNMA proteins are associated with this severe autoimmune disease is unclear. *PNMA* genes are predominantly expressed in the central nervous system and are ectopically expressed in some tumors. We show that *PNMA2*, which has been co-opted from a Ty3 retrotransposon, encodes a protein that is released from cells as non-enveloped virus-like capsids. Recombinant PNMA2 capsids injected into mice induce autoantibodies that preferentially bind external "spike" PNMA2 capsid epitopes, whereas a capsid-assembly-defective PNMA2 protein is not immunogenic. PNMA2 autoantibodies in cerebrospinal fluid of patients with anti-Ma2 paraneoplastic disease show similar preferential binding to spike capsid epitopes. PNMA2 capsid-injected mice develop learning and memory deficits. These observations suggest that PNMA2 capsids act as an extracellular antigen, capable of generating an autoimmune response that results in neurological deficits.

INTRODUCTION

The *PNMA* family of genes are predominately expressed in the brain,[1–4] but little is known about their biological function. *PNMA1-2* were first identified as genes encoding proteins that are targets of neuronal autoantibodies in blood and cerebrospinal fluid (CSF) from patients with paraneoplastic neurological syndromes.[1–3] Patients with elevated levels of PNMA1 (Ma1) or PNMA2 (Ma2) autoantibodies experience limbic/brainstem encephalitis and cerebellar degeneration.[5] These patients often present with solid peripheral tumors that are a potential source of paraneoplastic Ma antigen (PNMA) protein[1,3,6,7] and antibodies to PNMA proteins can be diagnostic of specific cancers.[8] Prognosis in this paraneoplastic syndrome is poor.[7] Moreover, recent studies have found that checkpoint inhibitors used to treat cancer can sometimes result in neurological deficits associated with Ma2 autoantibodies.[9,10] However, it has remained enigmatic why these proteins are associated with severe autoimmune disorders, but given the severity of disease, it is crucial to gain an understanding of the pathophysiology.

PNMA proteins are predicted to have retroviral Gag-homology domains.[11–13] Recent studies identified Gag-derived proteins co-opted from long terminal repeat (LTR) retrotransposons[11–14] that mediate an unexpected virus-like intercellular communication pathway.[15,16] These genes include the neuronal *Arc* genes that are critical for synaptic plasticity, memory, and cognition.[15–18] The Gag domain contained in LTR retrotransposons and retroviruses is necessary and sufficient to produce viral-like particles that package their own mRNA. The *Arc* gene, which was co-opted from a Ty3/mdg4 (formerly known as Ty3/gypsy) retrotransposon in the common ancestor of tetrapod vertebrates, encodes a protein that has retained virus-like biology.[16] Arc assembles into

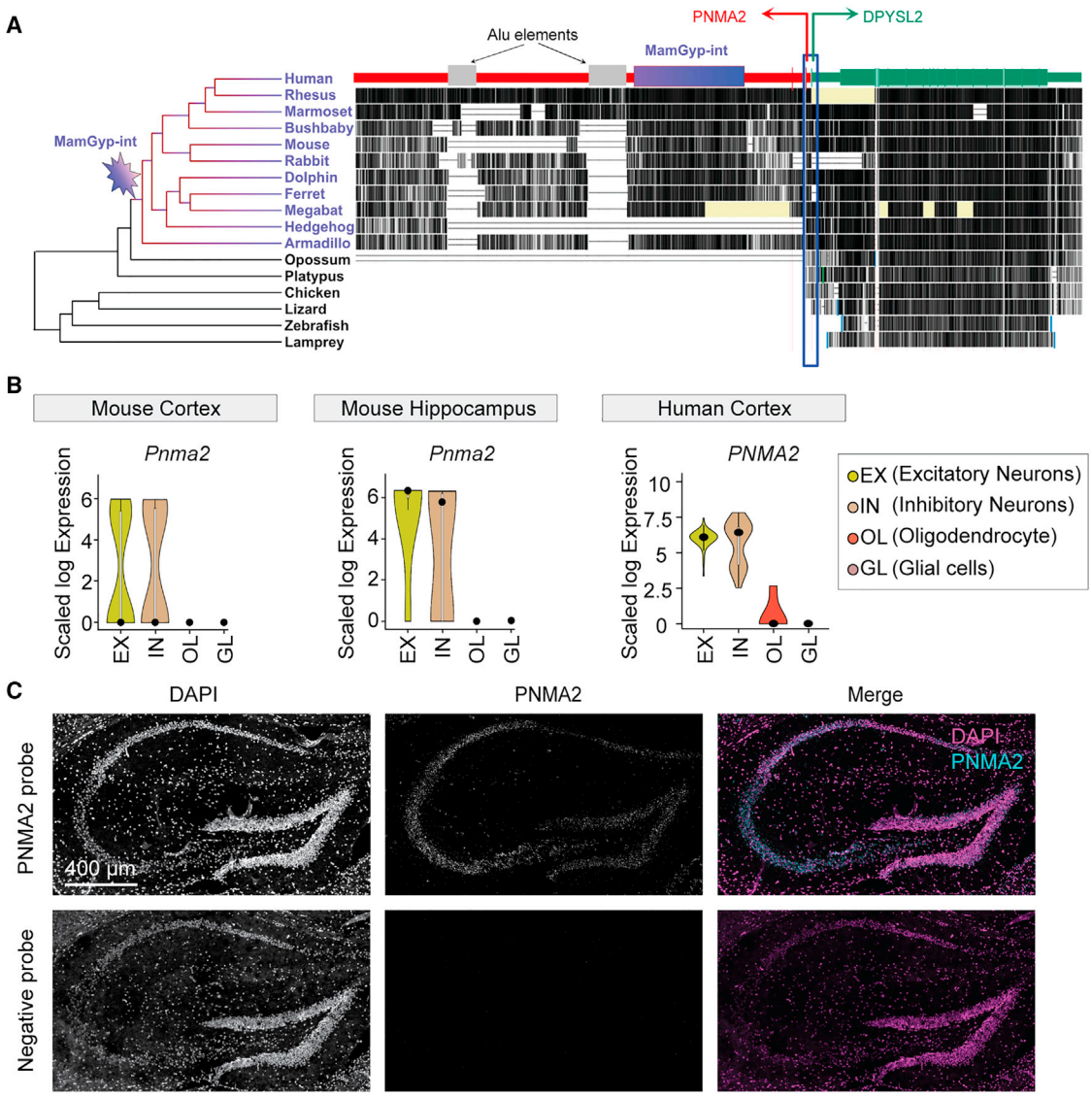

Figure 1. Ty3/mdg4 retrotransposon-derived *PNMA2* is expressed in mammalian neurons

(A) Evolution of PNMA2. Using data derived from the Vertebrate Multiz Alignment and Conservation track at the UCSC Genome Browser (hg38), we show the phylogenetic relationship (left) and sequence conservation (right) for a subset of vertebrate genomes across the mRNA sequence and shared promoter region of the *PNMA2* (red) and *DPYSL2* (green) genes. We find three transposable elements annotated by RepeatMasker within the *PNMA2* mRNA: a Mam-Gyp-int element (purple box) that gave rise to the Gag-like coding sequence, and two Alu elements (gray boxes) embedded within the 3′ UTR. The arrows depict the predicted transcription start sites for *PNMA2* and *DPYSL2*. The conservation track shows that *PNMA2* mRNA sequence is deeply conserved across placental mammals (except for the two Alu elements, which are primate-specific insertions), but not other vertebrates, while the *DPYSL2* and its promoter are conserved more deeply across vertebrate evolution.

(B) Violin plots visualizing the density and distribution of single-cell expression of PNMA2 mRNA in the mouse cortex (left panel), mouse hippocampus (middle panel), and human cortex (right panel). The solid black dots in each plot represent each lineage's median value of the PNMA2 expression.

(C) Representative image of single molecule fluorescent *in situ* hybridization (RNAscope) of *PNMA2* mRNA in the hippocampus of a 2-month-old mouse. Scale bars, 400 μm.

See also Figure S1.

virus-like capsids that are released from neurons in membrane-enveloped extracellular vesicles (EVs) that transfer RNA and protein cell-to-cell.[16] The *Drosophila* Arc (dArc) homologs also assemble capsids from a Gag domain that are released in EVs,[16,19] but originated independently from a distinct lineage of Ty3/mdg4 retrotransposons.[17,20] The Gag-like gene *PEG10*, which was derived from yet another lineage of Ty3/mdg4 retrotransposons during mammalian evolution, has also retained ancestral virus-like properties such as RNA binding, capsid formation, and release in EVs.[12,21–24] Together, these studies suggest that a diverse set of Gag genes have co-opted biochemical properties of ancestral retroelements to perform new host

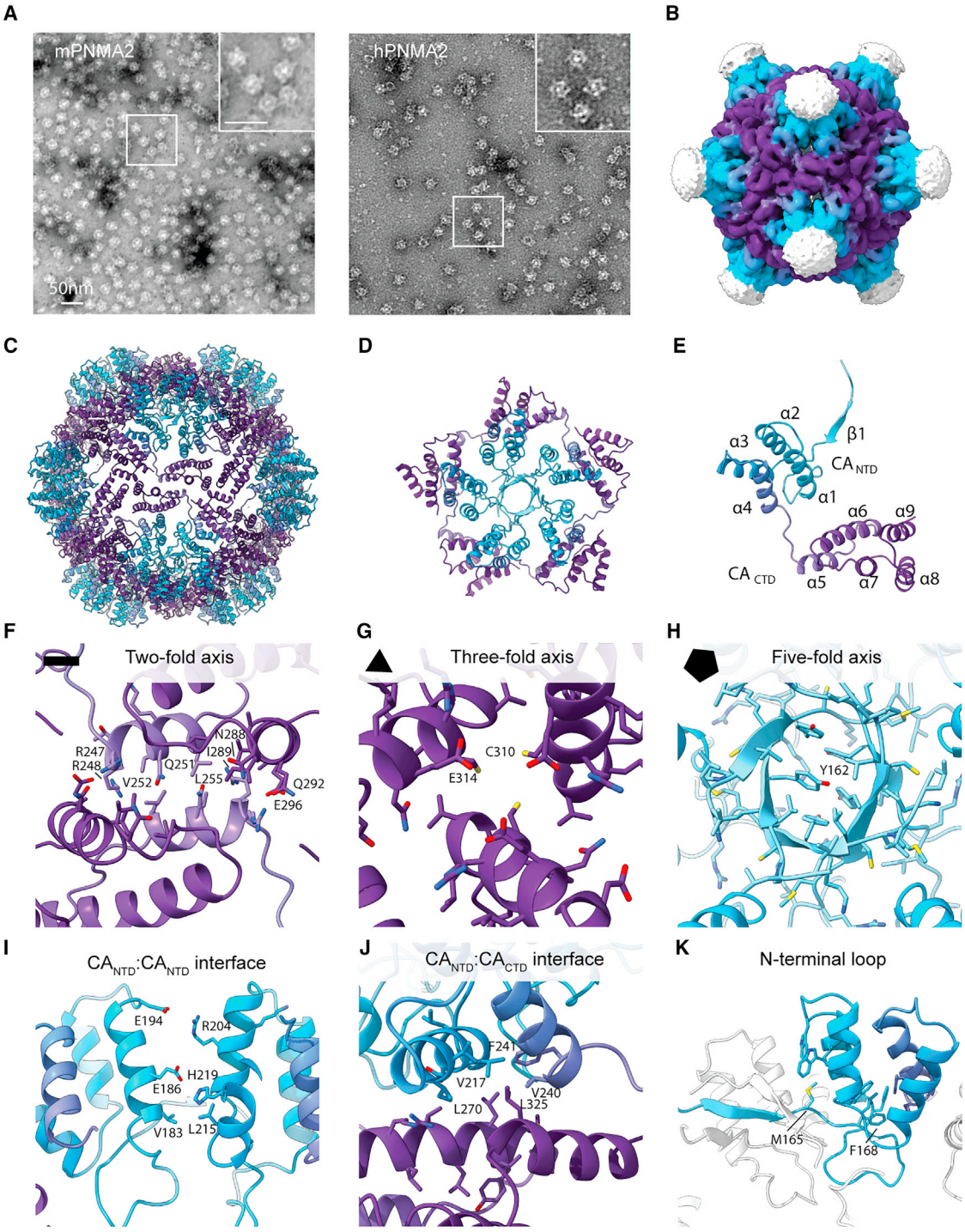

Figure 2. PNMA2 proteins self-assemble into T = 1 icosahedral virus-like capsids

(A) Representative negative-stained EM images of purified recombinant mouse PNMA2 (mPNMA2) capsids and human PNMA2 (hPNMA2) capsids. Scale bars, 50 nm.

(B) Cryo-EM-resolved surface representation of a mPNMA2 capsid, viewed down the 2-fold axis. The spike densities are not resolved.

(C) Atomic model of the T = 1 mPNMA2 capsid. CA_{NTD} is depicted in cyan and the CA_{CTD} in purple.

(D) External view of the isolated 5-fold capsomere.

(E) One of sixty mPNMA2 monomers required to form the T = 1 capsids.

(legend continued on next page)

functions.[25] However, their physiological functions and roles in human diseases are poorly characterized.

In this study, we investigated whether putative virus-like properties of PNMA proteins could explain their association with paraneoplastic neurological disorders. We concentrated on the *PNMA2* gene, which we find is normally exclusively and highly expressed in neurons. PNMA2 protein self-assembles into virus-like capsids that are released from cells as non-enveloped capsids. Based on these results, we posited that aberrant PNMA2 capsids released outside the central nervous system (CNS) may cause autoantibody generation. Consistent with this, mice injected with PNMA2 capsids produce strong autoantibody generation, even without adjuvant. Based on cryoelectron microscopy (cryo-EM)-derived atomic resolution structures of PNMA2 capsids, we designed PNMA2 mutants that are unable to form capsids. Injection of capsid mutant protein did not elicit autoantibody production, indicating that the fully assembled capsid is immunogenic. PNMA2 autoantibodies from injected mice and CSF from patients with anti-Ma2 paraneoplastic disease preferentially bind to exterior surface spike epitopes of PNMA2 capsids. PNMA2 capsids are also capable of inducing maturation of dendritic cells *in vitro*. Finally, mice injected with PNMA2 capsids develop significant deficits in fear learning and memory. Taken together, our results show that PNMA2 is a Gag-like protein that forms endogenous virus-like capsids that are released without a membrane. These capsids can trigger a robust immune response when ectopically expressed outside the CNS, which results in neurological deficits. The virus-like properties of PNMA2 protein may underlie some of the neurological symptoms associated with anti-Ma2 paraneoplastic disease.

RESULTS

PNMA2 evolved from a Ty3/mdg4 retrotransposon co-opted in the ancestor of placental mammals

Consistent with previous findings,[11,13] phylogenetic analysis shows that the *PNMA2* gene is conserved at an orthologous genomic position across all major lineages of placental mammals and was co-opted in the common ancestor of placental mammals ~100 million years ago, as it is absent from the genomes of marsupials and non-mammalian species (Figure 1A). The PNMA2 gene is composed of three exons. The first two are short noncoding exons interrupted by long introns, while the third exon encodes the open reading frame corresponding to the Gag-derived portion of an ancient MamGyp-int element of the Ty3/mdg4 superfamily. The predicted *PNMA2* promoter region is located only ~150 bp away from its nearest neighboring gene, *DPYSL2*, which is arranged in the opposite orientation relative to *PNMA2* (Figure 1A). This arrangement suggests that *PNMA2* and *DPYSL2* share a bidirectional promoter. Because the promoter region and the *DPYSL2* gene are more deeply conserved across vertebrate species than *PNMA2* (see sequence conservation track in Figure 1A), it is likely that the co-option of *PNMA2* was facilitated by the capture of a bidirectional promoter from pre-existing *DPYSL2*.

PNMA2 is expressed in mammalian neurons

To gain insight into *PNMA2* expression and localization, we first surveyed bulk RNA sequencing (RNA-seq) data from the genotype-tissue expression (GTEx) project,[26] which shows that *PNMA2* is highly and almost exclusively expressed in human brain tissue samples (GTEx: gtexportal.org/home/gene/ENSG00000240694) (Figure S1A). Next, we analyzed single-cell RNA sequencing datasets to examine *PNMA2* expression in human motor cortex, mouse cerebral cortex, and mouse hippocampus.[27–30] This analysis revealed that *PNMA2* mRNA is expressed in excitatory and inhibitory neurons, with very low expression in glia and oligodendrocyte lineages (Figure 1B). To confirm the RNA-seq data, we used single molecule fluorescent *in situ* hybridization (RNAscope) and found that *PNMA2* mRNA is abundant in mouse hippocampus (Figure 1C) and primary cultured hippocampal neurons (Figure S1B). To determine whether *PNMA2* expression pattern is conserved across species, we performed a cross species analysis using the human protein atlas platform. We found that the *PNMA2* expression pattern is conserved across mammals in distinct brain regions (Figure S1C). We also analyzed single-cell RNA-seq data from brain samples representing 33 anatomical regions from humans (n = 132), chimpanzees (n = 96), and macaques (n = 96).[31] These data show that *PNMA2* expression is conserved in gray matter areas of all three species, suggesting that the brain expression pattern is under strong selection (Figure S1D).

PNMA2 proteins self-assemble into virus-like capsids

Purified recombinant mammalian and dArc proteins spontaneously form virus-like capsids,[15,16] as do PNMA 3, 5, and 6a.[12] To determine whether PNMA2 also forms capsids, we affinity purified recombinant PNMA2 produced in an *E. coli* expression system and imaged the samples by negative stain EM. Purified mouse PNMA2 (mPNMA2) and human PNMA2 (hPNMA2) proteins, which have 78% amino acid identity, spontaneously form ordered virus-like capsids (Figure 2A). Recombinant mPNMA2 capsids were highly stable, even when treated with

(F) The 2-fold CA_{CTD} interface axis is formed between helices 5 and 7 through a hydrophobic interaction between V252 and L255, flanked by charged and neutral residues. We detect a potential salt bridge between R247 and Q292.
(G) Helix 8 constitutes the 3-fold CA_{CTD} interfaces, where E314 and C310 form the interface between the individual CA molecules.
(H) The 5-fold axis is constituted by residues 160–164 from each of the five CA molecules which form a short asymmetrical five-stranded beta-barrel, with one Y162 occupying the center of the capsomer.
(I) The CA_{NTD}:CA_{NTD} interfaces are formed between helices 1–3. Residues in helix 1, E186 and E194, may form salt bridges with R204 and H219 of helices 2 and 3, respectively.
(J) The CA_{NTD}:CA_{CTD} interface forms by docking of CA_{CTD} helix 6 residues L270 and L325 into a hydrophobic cavity formed by V217, F241, and V240 of helices 3 and 4 of the CA_{NTD}.
(K) The N-terminal residues F168 and M165 preceding helix 1 dock into two distinct hydrophobic grooves of CA_{NTD}.
See also Figures S2–S4, Table S1, and Videos S1, S2, and S3.

high concentrations of detergent (Figure S2). Using single particle cryo-EM, we reconstructed density maps of the entire icosahedral mPNMA2 capsid at a resolution of 3.2 Å, including local regions of the capsid surface after symmetry relaxation (Figures 2B and S3). mPNMA2 forms icosahedral capsids composed of 12 pentameric capsomeres and 60 individual mPNMA2 molecules, which have an outer diameter of ~200 Å and a triangulation number T = 1 (Figures 2C–2E). The protein shell of the capsid is ~30 Å thick. The high quality of the maps allowed us to build an atomic model of the mPNMA2 capsid (Figures 2C–2E; Video S1; Table S1). The capsid shell spans residues 157–336, which fold into a nine-helix bi-lobar CA domain structure, highly similar to Arc and Ty3 capsids[17,32] (Video S2). Both the CA_{NTD} and CA_{CTD} of mPNMA2 are compact helical domains with a hydrophobic core and hydrophilic surface. The 28 residues C-terminal to CA_{CTD} are located on the inside of the capsid shell, whereas the N-terminal 156 residues protrude from the center of the 5-fold capsomers to form a disordered spike (Figure 2B, 2D, and 2E). The 2-fold axis between the pentameric capsomeres is formed by helices 5 and 7 through a hydrophobic interaction between V252 and L255, flanked by charged and neutral residues. We detected a potential salt bridge between R247 and Q292 (Figure 2F). There is additional unresolved density at the inner side of the capsid, which appears to be an extension of helix 9 (Figures S4A–S4E). Helix 8 constitutes the 3-fold axis, where E314 and C310 form the interface between the individual CA molecules. While the three C310 residues are close enough to form alternating disulphide bonds, this region is less well resolved, and we do not observe density that could be assigned to coordination of ions (Figure 2G). Residues 160–164 from the five CA molecules form a short five-stranded beta barrel at the center of the 5-fold axis, with one Y162 occupying the center of the capsomer. Interestingly, the center of the 5-fold beta barrel is too small to accommodate the five Y162 residues symmetrically, enforcing an asymmetric 5-fold barrel (Figure 2H). By aligning the five monomeric CA molecules of the pentameric capsomeres to each other, we observe flexibility between the CA_{NTD} and CA_{CTD}, which may accommodate both the asymmetry in the center of the 5-fold capsomeres and alternating C310 disulfide bonds at the 3-fold axis (Video S3). The CA_{NTD}:CA_{NTD} interfaces are formed between helices 1–3 around the 5-fold capsomere. Residues E186 and E194 in helix 1 may form salt bridges with R204 and H219 of helices 2 and 3, respectively (Figure 2I). The CA_{NTD}:CA_{CTD} interface forms by docking of CA_{CTD} helix 6 residues L270 and L325 into a hydrophobic cavity formed by V217, F241 and V240 of helices 3 and 4 of the CA_{NTD} (Figure 2J). The N-terminal residues F168 and M165 preceding helix 1 dock into two distinct hydrophobic grooves of CA_{NTD} (Figure 2K).

The subunit assembly of the mPNMA2 capsid is very similar to the Ty3 retrotransposon capsid and the mature HIV-1 capsid, confirming the conservation of Gag-like capsid assembly (Figure S4F). However, unlike dArc1, mPNMA2 does not contain any conserved nucleic-acid-binding motifs in the capsid interior part of the protein. The electrostatic potential of the interior capsid shell reveals only one exposed positively charged patch located at the 2-fold symmetry axis. This interface is likely transiently shielded by a highly negatively charged motif in the putative extended C terminus of the protein (Figures S4G and S4H). These observations suggest that any interactions with oligonucleotides mediated by the CA domain and C-terminal residues are likely to be charge-based and non-specific. These data suggest that mPNMA2 forms retrovirus Gag-like T = 1 capsids that do not package specific nucleic acids.

PNMA2 is released from cells as non-enveloped capsids

Retrovirus capsids are released from cells as membrane-enveloped particles, similar to EVs. Arc protein is also released in EVs.[16] To determine whether mPNMA2 is released from cells, we harvested media from primary cultured rat cortical neurons and fractionated the media using size-exclusion chromatography. PNMA2 protein was isolated in early fractions that are also enriched with canonical EV proteins such as the ESCRT protein ALIX (Figure 3A). To determine whether released PNMA2 protein is enveloped by a membrane, we performed a proteinase K protection assay. Surprisingly, PNMA2 protein was highly degraded by proteinase K even without detergent present, unlike EV proteins, suggesting a lack of membrane protection (Figures 3B and 3C). These results contrasted with endogenous Arc protein release from neurons, which showed significant protection from proteinase K (Figures 3B and 3C). To further determine whether PNMA2 is released in EV fractions, we used iodixanol gradient ultracentrifugation and found that endogenous PNMA2 protein is enriched in a different fraction (fraction 6) than neuronal EV proteins (fraction 3), indicating released PNMA2 differs in density from EVs (Figure 3D). Moreover, capsid structures were observed in iodixanol fraction 6, as determined by negative-staining EM (Figure 3E). To measure enough capsids to determine average size, myc-mPNMA2 was transfected into HEK293T cells (Figures S5A–S5D) and media processed using iodixanol ultracentrifugation. Capsids isolated from iodixanol fraction 6 and imaged on EM grids showed an average size (~21 nm) similar to capsids from purified recombinant mPNMA2 protein (Figure S5E). We did not observe any membrane envelopes surrounding capsids in these EM images.

Patients with anti-Ma2 paraneoplastic syndrome predominately present with testis and lung cancer[6] and *PNMA2* is highly expressed in various tumors (Figure S1E). To test whether tumor cells release hPNMA2 protein, we used a human testis cancer cell line (NTERA-2) and human lung cancer cell line (NCI-H378) that express high levels of hPNMA2.[33,34] We harvested cell culture media after 24 h and performed size exclusion chromatography. hPNMA2 is expressed and released from NTERA-2 (Figure 3F) and NCI-H378 cells (Figure S5F). As we observed for neurons, hPNMA2 protein released from these cell lines was not protected from proteinase K degradation (Figures 3G, S5G, and S5H), indicating release as non-enveloped capsids. Interestingly, the release of PNMA2 seems to be cell type specific as mPNMA2 overexpressed in the murine colorectal carcinoma cell line MC-38 was not released (Figure S5I).

To determine whether mPNMA2 release requires assembled capsids, we designed point mutations predicted to disrupt the 5-fold axis (Y162A [Y/A]) and the CA_{NTD}-CA_{CTD} capsid interface (L270Q/L325Q [L/Q]) between mPNMA2 subunits (Figures 2H and 2J). Similar mutations in the CA_{NTD}-CA_{CTD} interfaces disrupt retrovirus capsid assembly.[35] As predicted, purified mPNMA2

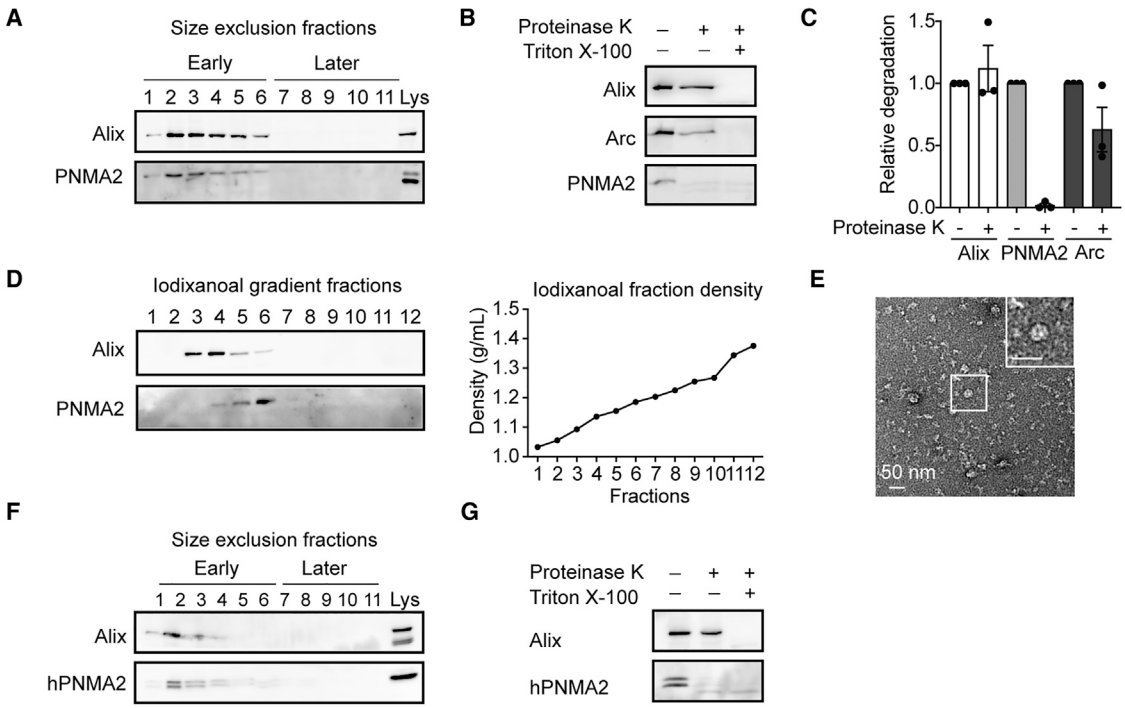

Figure 3. Endogenous PNMA2 is released from cells as non-enveloped capsids

(A) Media was collected from primary cultured rat cortical neurons (DIV15–16) and fractionated using size exclusion chromatography (SEC). Fractions were run on a gel and blotted for PNMA2 and ALIX, a canonical EV marker. PNMA2 protein is released in early fractions that contain EV proteins.

(B) The early fractions (1–4) from primary cultured cortical neuronal media SEC were pooled and blotted for Arc, PNMA2, and ALIX. Fractions were incubated with proteinase K (7 μg/mL) with or without detergent present (1% Triton X-100) for 10 min. Representative western blots show that PNMA2 protein was sensitive to proteinase K degradation without detergent present.

(C) Quantification of western blots in (B) (n = 3 cultures). Error bars indicate mean ± SEM.

(D) The early SEC fractions (1–4) from primary cultured cortical neuronal media were further fractionated using ultracentrifugation, and an iodixanol gradient was used to separate proteins by density and size. PNMA2 protein was enriched in fraction 6, while ALIX was enriched in fractions 3 and 4.

(E) Representative negative-stained EM image of non-enveloped PNMA2 capsids isolated from iodixanol gradient fraction 6 in (D). Scale bars, 50 nm.

(F) Media was collected from cultured NTERA-2 testis cancer cells and fractionated using SEC. Fractions were run on a gel and blotted for hPNMA2 and ALIX. hPNMA2 is released in early fractions that contain EV proteins.

(G) The early SEC fractions (1–3) from NTERA-2 media were pooled and blotted for hPNMA2, and ALIX. Fractions were incubated with proteinase K (7 μg/mL) with or without 1% Triton X-100 for 10 min. Representative western blots show that hPNMA2 protein was sensitive to proteinase K degradation without detergent present.

See also Figure S5.

Y/A and mPNMA2 L/Q proteins were unable to form capsids as analyzed by size exclusion chromatography, negative-stain EM, and mass photometry (Figures 4A–4C). mPNMA2, mPNMA2 L/Q, or mPNMA2 Y/A were expressed in HEK293T cells and protein release was measured. The relative release of mPNMA2 L/Q and Y/A were significantly reduced compared with wild-type (WT) protein (Figures 4D and 4E). Together, these data show that PNMA2 is released from cells as non-enveloped virus-like capsids.

PNMA2 capsids induce autoantibody production

We next examined whether PNMA2's virus-like properties could be responsible for inducing an autoimmune response. Since PNMA2 appears to be exclusively expressed in neurons of the CNS (Figures 1B and S1), we hypothesized that aberrant expression of PNMA2 in tumor cells (Figure S1E) and release of capsids outside of the CNS may be immunogenic. Virus capsids can induce a stronger immune response than soluble proteins due to the capsid's influence on antigen transport, adaptive immune response, avidity, and cross-presentation.[36–39] Thus, the ability of PNMA2 protein to form capsids that are released without membranes could explain its immunogenicity. To assess the immunogenicity of mPNMA2 capsids, we injected mice with 5 μg of purified recombinant mPNMA2 capsids without adjuvant and collected blood 3 weeks after injection. mPNMA2-capsid-injected mice produced high titers of antibodies that bound mPNMA2 capsids, as assessed by ELISA (Figure 5A) and by immunogold EM (Figure 5B). However, mice injected with 5 μg of purified mPNMA2 L/Q capsid mutant protein did not produce mPNMA2 L/Q-specific antibodies (Figure 5A). A second injection of 5 μg mPNMA2 L/Q 3 weeks after the first injection, which could prime the immune system, also failed to induce autoantibody production further indicating a lack of immunogenicity of non-capsid forming mPNMA2 protein (Figure 5C).

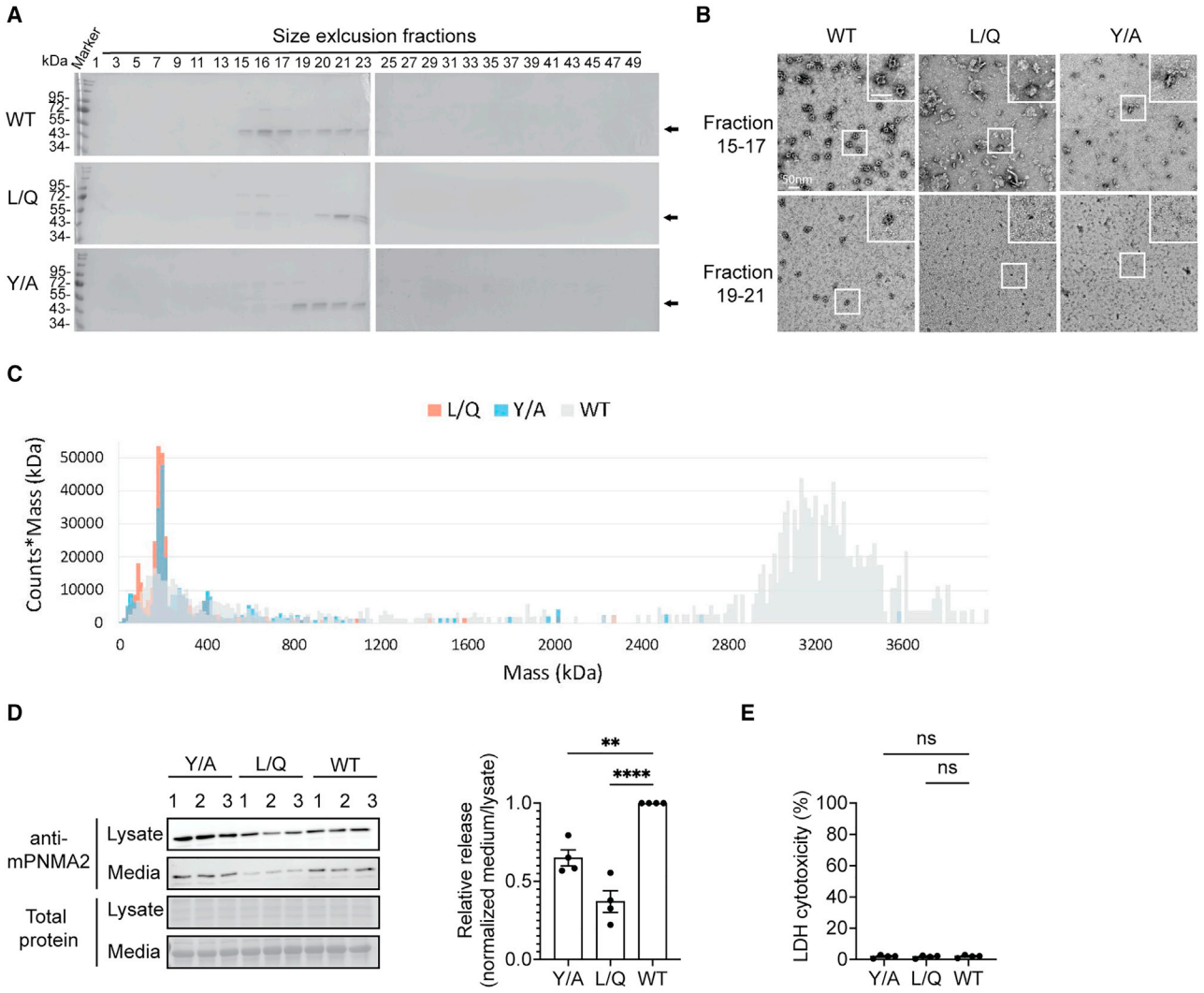

Figure 4. mPNMA2 capsid assembly mutants show reduced release from cells

(A) Representative Coomassie SDS-PAGE gels show peak fractions eluted from the SEC column for purified mPNMA2 WT, mPNMA2 L270Q/L325Q (L/Q), and mPNMA2 Y162A (Y/A) mutant proteins. mPNMA2 L/Q and Y/A proteins are shifted to later fractions, indicating lack of assembled capsids.

(B) Representative negative-stained EM images of mPNMA2 WT, L/Q, and Y/A proteins from pooled SEC fractions 15–17 and 19–21. mPNMA2 L/Q and Y/A proteins do not form capsids. Scale bars, 50 nm.

(C) Mass distribution histograms of purified mPNMA2, L/Q, and Y/A proteins, measured by mass photometry. mPNMA2 L/Q and Y/A proteins are not found in high-molecular-weight assemblies (>3,000 kDa).

(D) Western blot of mPNMA2 WT, L/Q, and Y/A expression in cell lysates and media from transfected HEK293T cells. L/Q and Y/A proteins are released less than WT mPNMA2 protein (n = 4 cultures for each group; ****One-way ANOVA with Dunnett's multiple comparisons, $p < 0.0001$. WT vs. Y/A: **$p = 0.0014$; WT vs. L/Q: ****$p < 0.0001$).

(E) LDH cytotoxicity assay to test the viability of HEK293T cells in (D). No differences in toxicity were observed (one-way ANOVA with Dunnett's multiple comparisons, $p = 0.9271$; WT vs. Y/A: $p = 0.9925$; WT vs. L/Q: $p = 0.9028$). Error bars indicate mean ± SEM.

The structure of mPNMA2 capsids suggests that the exposed spikes may be more immunogenic than the capsid body since these residues are more likely to be exposed to adaptive immune cells.[40,41] To test this idea, we purified the N-terminal region of mPNMA2 capsids (the spike aa 1–170) and the main capsid shell (aa 171–365) (Figure 5D). Autoantibodies from capsid-injected mice preferentially bound the N-terminal spike fragment (Figure 5D). To determine whether PNMA2 autoantibodies from paraneoplastic patients bind hPNMA2 capsids, we obtained CSF samples from patients diagnosed with anti-Ma2 paraneoplastic syndrome (see STAR Methods for patient information) and control CSF samples (see STAR Methods). Using an ELISA coated with recombinant hPNMA2 capsids, we confirmed that paraneoplastic patient CSF contains high levels of PNMA2 autoantibodies that are capable of binding capsids, whereas control patient CSF do not have PNMA2 autoantibodies (Figure 5E). PNMA2-specific antibodies in paraneoplastic patient CSF also robustly labeled hPNMA2 capsids, as determined by

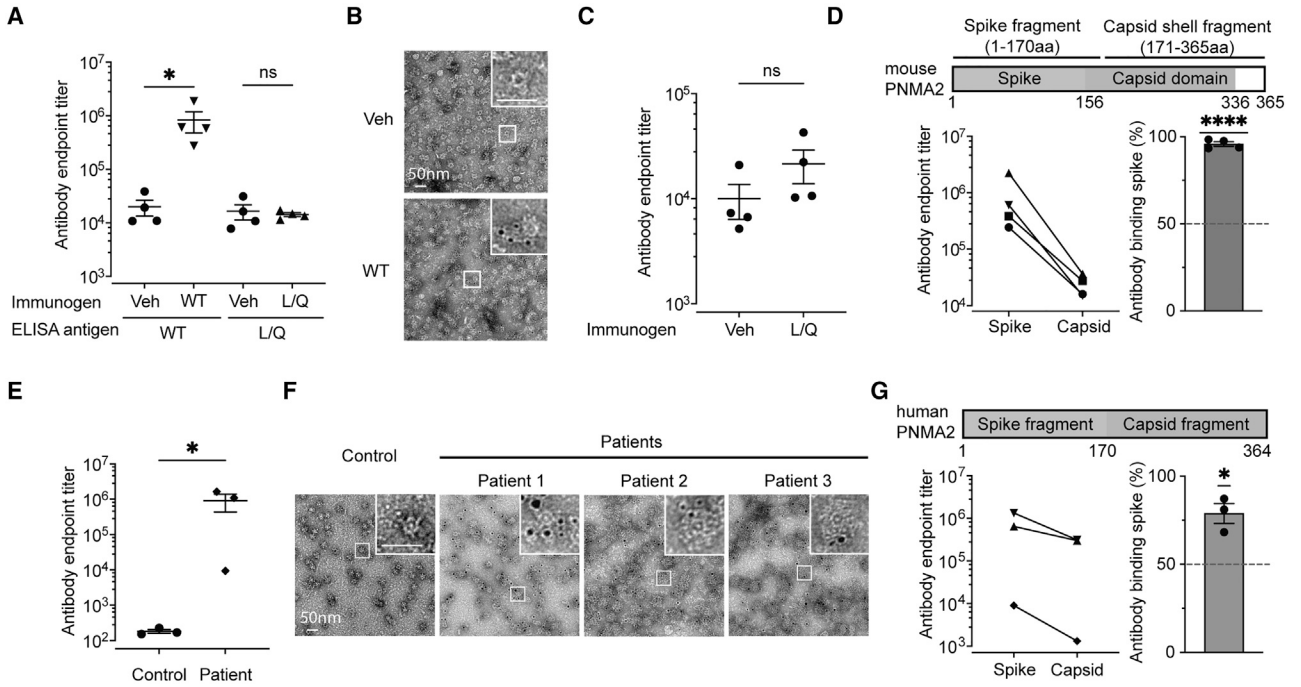

Figure 5. PNMA2 capsids induce autoantibody production

(A) Mice were injected intraperitoneally with vehicle (n = 4), 5 μg purified mPNMA2 capsids (n = 4) or 5 μg mPNMA2 L/Q protein (n = 4) and blood sera collected 3 weeks after injections. Sera were analyzed for antibody production using ELISA, using 2 μg/mL mPNMA2 WT capsids or mPNMA2 L/Q protein coated on the plates as the antigen. mPNMA2 capsid-injected mice produced robust PNMA2 autoantibodies, whereas vehicle and mPNMA2 L/Q injections did not elicit autoantibody production (Mann-Whitney test. Vehicle vs. WT [using WT capsids as antigen]: $p = 0.0286$; vehicle vs. L/Q [using L/Q as antigen]: $p = 0.8857$).

(B) Representative negative-stained EM images of purified mPNMA2 capsids immunogold labeled with mouse PNMA2 autoantibodies in serum collected from mPNMA2 capsid-injected mice. Scale bars, 50 nm.

(C) Mice sera collected 3 weeks after the second injection of vehicle or 5 μg mPNMA2 L/Q were analyzed for antibodies against mPNMA2 L/Q protein by ELISA. Antibodies were not produced after the second injection of L/Q. (Mann-Whitney test, $p = 0.1143$).

(D) Purified mPNMA2 spike fragments and capsid shell fragments (see schematic) were used as ELISA antigens to determine the epitopes of PNMA2 autoantibodies from mPNMA2 capsid-injected mice. The schematic shows mPNMA2 protein regions located on the spike and the capsid domains of capsids, as determined by the cryo-EM structure. PNMA2 autoantibodies preferentially bind to the spike fragments (****one sample t test, $p < 0.0001$, null hypothesis of 50% binding).

(E) An ELISA, using purified hPNMA2 capsids as the antigen, was used to quantify PNMA2 autoantibodies in CSF from patients diagnosed with or without PNMA2-related paraneoplastic neurological syndrome (n = 3 for each group, *Mann-Whitney test, $p = 0.05$).

(F) Representative negative-stained EM images of hPNMA2 capsids labeled with immunogold using CSF from control or paraneoplastic patients. Scale bars, 50 nm.

(G) ELISAs using hPNMA2 spike and capsid shell fragments as antigens show patient CSF PNMA2 autoantibodies preferentially bind to the spike fragment (*one sample t test, $p = 0.0356$, null hypothesis of 50% binding). Error bars indicate mean ± SEM.

Abbreviations are as follows: WT, wild type; L/Q, L270QL325Q; Veh, vehicle.

immunogold EM (Figure 5F). Paraneoplastic patient CSF PNMA2 autoantibodies preferentially bound N-terminal spike epitopes predicted to be on the exterior surface of hPNMA2 capsids (Figure 5G), similar to autoantibodies produced in capsid-injected mice. Taken together, these data support the hypothesis that PNMA2 autoantibodies are generated due to the high immunogenicity of PNMA2 virus-like capsids.

mPNMA2 capsids promote maturation of dendritic cells

To gain insight into how PNMA2 capsids induce an immune response, we assessed whether mPNMA2 can induce the maturation of bone-marrow-derived dendritic cells (BMDCs) *in vitro*. DCs play a central role in the initiation of the adaptive immune response following exposure to pathogen-associated or danger-associated molecular patterns.[42] After activation, DCs mature and upregulate key surface co-stimulatory molecules such as CD80, CD83, and CD86, which facilitate T cell activation.[43] Helper T cells can then activate B cells in draining lymph nodes and spleen, leading to robust antibody generation.[44] BMDCs were generated by culturing bone marrow extracted from WT mice for 7 days and then stimulated with either LPS (positive control), purified WT mPNMA2 capsid protein, proteinase K pre-treated WT mPNMA2 capsids or L/Q mPNMA2 protein (Figures 6 and S6). All mPNMA2 conditions resulted in a dose-dependent increase in the frequency of matured ($CD11c^{+}MHCII^{++}$) BMDCs (Figures 6A and S6A) and induced expression of the costimulatory receptors CD80, CD83, and CD86 (Figures 6B and S6B–S6D). However, pretreatment of capsids with proteinase K significantly blunted the induction of the costimulatory receptors (Figures S6B–S6D). Cytokine profiling demonstrated BMDCs

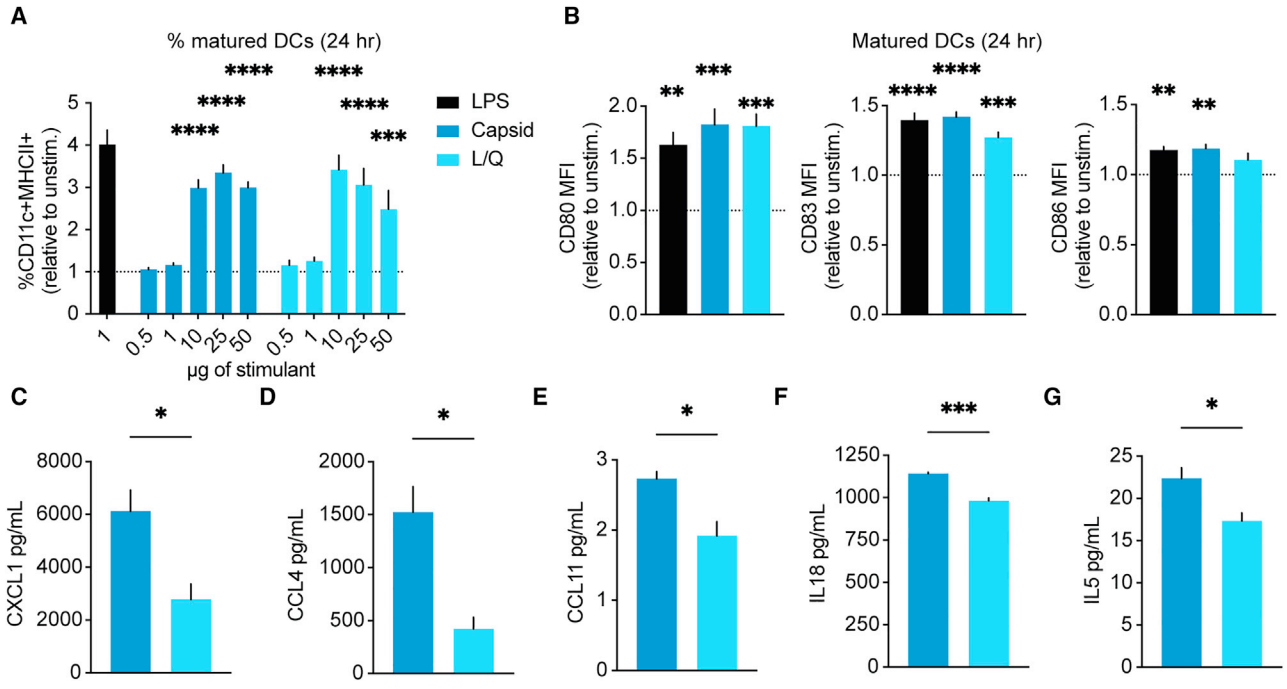

Figure 6. mPNMA2 capsids activate bone-marrow-derived dendritic cells

(A) Murine bone marrow cells were isolated and cultured with 20 ng/mL GM-CSF for 7 days to generate bone-marrow-derived dendritic cells (BMDCs), which were then incubated with varying concentrations of LPS, mPNMA2 capsids, or L/Q mPNMA2 protein for 24 h prior to flow cytometric analysis. Data show quantification of matured ($CD11c^{+}MHCII^{++}$) BMDC following stimulation, graphed as fold increase relative to unstimulated BMDC of the same experiment. n = 4 independent experiments. Both WT and L/Q mPNMA2 protein activates BMDCs.

(B) Mean fluorescence intensity (MFI) of CD80 (left), CD83 (middle), and CD86 (right) within the matured BMDC population graphed as fold increase relative to unstimulated BMDC of each independent experiment with 50 μg antigen stimulation. Both WT and L/Q mPNMA2 protein induce costimulatory receptor expression.

(C–G) Cell culture supernatants of BMDC from (A) were collected and analyzed for expression of cytokines CXCL1 (C), CCL4 (D), CCL11 (E), IL18 (F), IL5 (G) using the ProcartaPlex immunoassay. n = 3 biological replicates. WT mPNMA2 capsids induce significantly higher levels of cytokine release than L/Q mPNMA2 protein. Error bars: mean ± SEM. Statistics were determined using a two-way ANOVA with Dunnett's multiple comparisons test using unstimulated values as a control (A), one-way ANOVA with Dunnett's multiple comparisons test using unstimulated values as a control (B) or unpaired t test (C–G), *$p < 0.05$, ***$p < 0.001$, ****$p < 0.0001$.

See also Figure S6.

treated with WT capsids induced significantly higher levels of key inflammatory cytokines than L/Q mutant capsid protein (Figures 6C–6G), suggesting assembled PNMA2 capsids might drive a stronger adaptive immune response. These data suggest that assembled mPNMA2 capsids can robustly stimulate DCs to initiate the adaptive immune response.

Immunization with mPNMA2 capsids induces learning and memory deficits in mice

Patients with anti-Ma2 paraneoplastic neurological syndrome present with neurological symptoms that include learning and memory deficits.[7,45] To determine whether mice immunized with PNMA2 capsids develop neurological deficits, we used a mouse contextual fear conditioning paradigm[46] (Figure 7A). 3 months after the second injection of mPNMA2 WT capsids or L/Q mutant protein, mice were placed in a chamber that included contextual cues and then given four mild electric foot shocks (1 min inter-trial-interval [ITI]). Fear was indexed by freezing behavior.[46] Mice injected with mPNMA2 capsids showed deficits in the ability to acquire contextual fear, as compared with non-injected and L/Q injected mice (Figure 7B), suggesting a deficit in the ability to learn the association between the context and foot shock. Importantly, this could not be explained by a reduced sensitivity to pain, as mPNMA2 capsid mice showed similar levels of motion in response to the shock (Figure 7C). To test memory, we returned mice to the original training chamber 24 h after training and measured freezing levels over a 3-min period. mPNMA2-capsid-injected mice showed significantly less freezing than non-injected and L/Q-injected mice (Figure 7D), indicating that the learning deficits persisted with low levels of memory retention. These data show that mPNMA2 capsid-injected mice develop learning and memory deficits reminiscent of neurological symptoms observed in Ma2 patients.[7]

To determine whether these mice developed brain pathology or neuroinflammation, we used immunohistochemistry for markers of astrocytes, microglia, or neurons and found no gross differences in their number or morphology (Figures S7A–S7C). We also did not detect T or B cell infiltration in the brains of capsid-injected mice (Figures S7D and S7E). Together, these data suggest that mPNMA2-capsid-injected mice develop

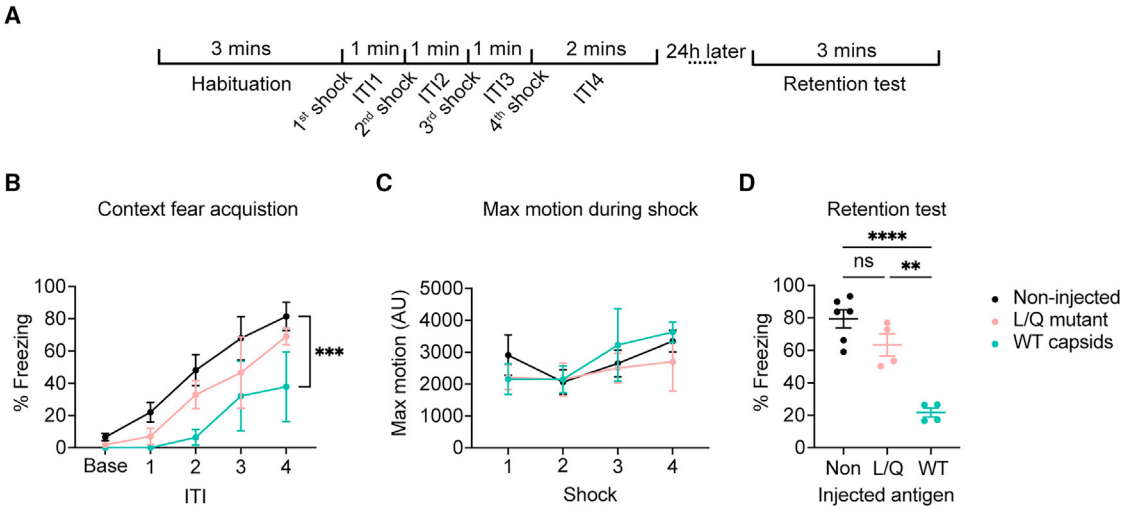

Figure 7. mPNMA2 capsid-injected mice develop learning and memory deficits

(A) Schematic of the fear conditioning behavior paradigm. Mice were injected with 5 μg of mPNMA2 capsids or capsid mutant L/Q mPNMA2 protein, followed by a booster injection of 5 μg protein 3 weeks later. 3 months after the second injection, mice were conditioned to associate mild foot shocks with a specific context. Abbreviation is as follows: ITI, inter-trial interval.

(B) We measured the percentage of mice freezing during fear conditioning. mPNMA2 capsid-injected mice showed decreased freezing during the training. Baseline was assessed 30 s before the 1st shock. ITI 1–4 were assessed as 30 s bins from the 30th second after the shock. Two-way ANOVA with Tukey's multiple comparisons test. Main effect, shock: $F(4, 55) = 15.67$, ****$p < 0.0001$; injected antigen: $F(2, 55) = 9.691$, ***$p = 0.0002$; non-injected vs. capsids, ***$p = 0.0001$; non-injected vs. L/Q mutant, $p = 0.1190$; capsids vs. L/Q mutant, $p = 0.0846$.

Abbreviations are as follows: Base, baseline; ITI, inter-trial interval.

(C) The maximum motion of mice during the shock (measured 5 s from the beginning of shock presentation). There was no difference between PNMA2 capsid and L/Q-injected mice, indicating normal pain perception of the shock. Two-way ANOVA. Main effect, shock: $F(3, 44) = 2.110$, $p = 0.1125$; injected antigen: $F(2, 44) = 0.5415$, $p = 0.5857$.

(D) A memory retention test was performed 24 h after training. mPNMA2 capsid-injected mice showed a significant decrease in freezing, compared with non-injected and L/Q-injected mice, which showed robust memory recall. One-way ANOVA test with Tukey's multiple comparisons test, ****$p < 0.0001$. Non-injected vs. L/Q mutant: $p = 0.1405$; non-injected vs. capsids: ****$p < 0.0001$; L/Q mutant vs. capsids: **$p = 0.0012$. (B–D) Non-injected group: n = 6 mice (3 male + 3 female); L/Q and capsids injected group: n = 4 mice (2 male + 2 female). Error bars indicate mean ± SEM.

See also Figure S7.

neurological deficits without overt brain inflammation or pathology, recapitulating some aspects of Ma2 paraneoplastic syndrome.

DISCUSSION

The discovery that Arc proteins form virus-like capsids intimated that other co-opted Gag-derived proteins might also retain the ability to form capsids and that this property may have been repurposed repeatedly during evolution to function in intercellular communication.[12,15,16] Indeed, other predicted Gag-like genes, such as *PEG10* and the *PNMA* genes, encode proteins that also form virus-like particles.[12] Here, we found that PNMA2 protein, which is highly expressed in mammalian cortex and hippocampus, forms small non-enveloped virus-like capsids that are released from cells. Thus, there is a repertoire of different mammalian endogenous virus-like capsids that have been evolutionarily repurposed from retrotransposons,[25] which have distinct biophysical properties and functions.

PNMA2 forms non-enveloped virus-like capsids

The structure of the mPNMA2 CA domain and the higher-order oligomers that form the capsid is remarkably similar to those previously reported for dArc1/2, Ty3 retrotransposon and mature HIV-1 capsids.[17,32,47] This supports the idea that PNMA2, similar to Arc, originated from a retrotransposon ancestor and that the ability to form capsids has been under strong purifying selection. However, the mPNMA2 capsids are considerably smaller (T = 1, outer diameter of ~20 nm) than those of dArc (outer diameter of ~37 nm) or Ty3 (outer diameter of ~50 nm). If the RNA packing density is similar to Ty3,[32] mPNMA2 capsids would only be able to accommodate ~350 nucleotides. The C-terminal region of mPNMA2 has diverged from those in dArc and Ty3, where the internal C-terminal zinc-finger motif from Ty3 and dArc1 is replaced by 30 highly acidic residues that extend helix 9 and dock against a positively charged patch at the 2-fold position on the inner capsid surface. These observations, along with the smaller size of the mPNMA2 capsid, make it unlikely that mPNMA2 capsids transport nucleic acids in the same way as Arc or typical retroviral capsids. However, it is possible that mPNMA2 forms larger capsids under certain conditions, perhaps even as heteromeric capsids with other PNMA family members, which is conceivable considering the structural flexibility of the mPNMA2 capsid and retrotransposon/retrovirus capsids in general. Capsid expansion would not only allow an increase in capsid capacity but would also allow the inclusion of additional hexameric

capsomers that could expose putative nucleic-acid-binding sites (since the acidic C terminus may be oriented differently in hexameric capsomers) or to package additional cofactors that could specifically encapsulate nucleic acids. The ~150 N-terminal residues of mPNMA2 form the capsid exterior spikes and are predicted to fold into two interconnected structured domains (Figure S4I), but the flexibility of this region prevented us determining a structure. Recent computational approaches suggest that the spike may also contain an RNA-binding domain, at least in the monomeric form.[48] Determining the structure and function of this region will be critical as these spikes are likely to mediate protein-protein or protein-lipid interactions, and possibly RNA interactions, that facilitate release, uptake, and immune system activation.

In contrast to Arc release in EVs,[16,25] we found that PNMA2 is released from cells as non-enveloped capsids. These capsids are released via an unknown secretory pathway, possibly through non-canonical autophagy or lysosomal pathways.[49,50] Some viruses, such as adenoviruses and adeno-associated viruses (AAVs), are also released without membranes from cells. However, the cell biology and mechanisms of non-enveloped capsid release and uptake remain obscure.[51] Since AAVs are used in current gene therapy applications and endogenous capsids may also be harnessed for gene delivery,[12] understanding how non-enveloped PNMA2 capsids are released and taken up by mammalian cells may facilitate gene therapy applications.

PNMA2 capsids are highly immunogenic

Assembled mPNMA2 capsids injected into mice result in robust generation of autoantibodies, even without adjuvant, that preferentially bind to external spike epitopes on capsids. Conversely, mice injected with capsid-disrupting L/Q mutant mPNMA2 protein showed no autoantibody response, highlighting the specific immunogenicity of fully assembled capsids. Patient PNMA2 autoantibodies from CSF also preferentially bind to external spike epitopes on hPNMA2 capsids, which corroborates previous observations in Ma2 patients: the N-terminal region (1–198 aa) of PNMA2 was recognized by all patients' sera, while a C-terminal region (214–435 aa) was identified in only 20 of 29 sera, and reactivity was consistently weaker.[1] PNMA2 capsids may be more stable in blood than monomeric protein, especially since these capsids are highly detergent resistant. Bona fide virus capsids induce strong immune responses through a variety of mechanisms, including increased B cell avidity[38,39] and via specific pattern recognition mechanisms (such as TRIM5 for HIV).[52] Our data indicate that PNMA2 capsids may trigger a complex immune response, including maturation of DCs. DC maturation, induced by exposure to pathogen-associated and danger-associated molecular patterns,[42] initiates expression of surface receptors and release of cytokines capable of assisting in activation of T cells.[43] The unique combination of costimulatory receptor expression and cytokine release, which is determined by the stimulus received, impacts the phenotype of downstream immune responses.[53] Both WT and L/Q capsids induced maturation of DCs, as measured by surface marker expression and cytokine release; however, the magnitude of cytokine release was lower in DCs incubated with L/Q protein for several immunostimulatory cytokines and chemokines. This difference in cytokine release may explain why injected assembled capsids trigger autoantibody production, while injected L/Q protein does not. The capsid structures of repurposed Gag proteins like PNMA2 and Arc are strikingly similar to infectious retroviruses; thus, we speculate that capsids formed by endogenous retroviruses (ERVs) may also be capable of eliciting strong immune responses. Indeed, ERVs have been implicated in various human diseases such as cancer and neurodegeneration.[54,55]

PNMA2 capsids may underlie anti-Ma2 paraneoplastic neurological syndrome

The precise role of immune processes in the heterogeneous paraneoplastic neurological syndromes remain poorly characterized but are thought to be primarily mediated by T cell-induced inflammatory responses. However, autoantibodies to intracellular neuronal proteins such as Hu can be taken up by neurons in brain slices, leading to neuronal death.[56] Moreover, autoantibodies to surface neuronal and synaptic proteins such as the NMDA-type glutamate receptor can directly cause specific neurological symptoms such as limbic encephalitis.[57] Patients with anti-Ma2 autoantibodies predominantly present with neurological deficits[7,58] and the neurological symptoms associated with anti-Ma2 paraneoplastic syndrome are distinct from other paraneoplastic syndromes, especially as compared with other intracellular antigens such as Yo.[7] Brain pathology studies (autopsy or biopsy of Ma2 patient brain tissue), which include the patients in this study, found perivascular lymphocytic cuffing and interstitial infiltrates of lymphocytes (mainly T cells, with smaller amounts of B cells) with variable gliosis, microglial activation, and neuronal degeneration.[7] Since normal expression of *PNMA2* is restricted to the brain, we speculate that an immune response may be elicited when tumors release high amounts of PNMA2 capsids outside the CNS. Indeed, our data suggest that PNMA2 is not a conventional intracellular neuronal antigen such as Hu or Yo. Based on our release assays, tumors that efficiently release PNMA2 (such as lung and testicular cancers) have a much higher probability of being associated with PNMA2 autoantibodies—a prediction that is consistent with clinical experience.[7] Whether autoantibody production correlates with overall PNMA2 levels or amount of release from tumors remains to be determined.

We find that capsid-injected mice develop learning and memory deficits without overt brain pathology or inflammation. This is in contrast to anti-Ma2 paraneoplastic patients, which show neuroinflammation in the brain. Thus, acute PNMA2 capsid injections do not fully model the human disease. Given that secreted PNMA2 capsids lack a membrane envelope, PNMA2 autoantibodies in patient CSF could bind to PNMA2 capsids released under physiological conditions and interfere with putative intercellular signaling functions of PNMA2. However, we do not have causal evidence that PNMA2 autoantibodies trigger neurological deficits and future studies will be needed to determine the normal function of PNMA2. Attempts to model paraneoplastic neurological syndromes in animal models have been difficult, partly due to lack of antigen immunogenicity or the development of neurological deficits.[59] PNMA2 capsid-injected mice show some clinical features of anti-Ma2 paraneoplastic syndrome and offers an opportunity to determine the underlying pathophysiology.

Conclusions

Our data indicate that endogenous capsid forming proteins can trigger an autoimmune response. However, PNMA2 capsids may be unique as they are released without membranes and expression is normally restricted to the brain, suggesting they could be immune privileged under normal conditions. The structural information we uncovered on PNMA2 capsids may ultimately provide a resource to design capsids that mitigate an autoimmune response, as Gag-like proteins have recently been proposed as new delivery vehicles for gene therapy.[12]

We have shown that PNMA2 forms virus-like capsids that are normally released from cells as non-enveloped particles. PNMA2 is primarily and highly expressed in the mammalian brain, with conserved expression pattern across species, but the biological function of PNMA2 remains unknown. We speculate that the virus-like properties of PNMA2 are important for its function in the brain. Since PNMA2 capsids do not seem to encapsulate specific nucleic acid, their precise signaling role will likely uncover novel processes underlying intercellular communication. Future studies will determine the function of PNMA2 capsids and whether other PNMA proteins form virus-like capsids that are released as non-enveloped particles in the nervous system.

Limitations of the study

While our results show that mPNMA2 capsids elicit an autoimmune response that ultimately results in learning deficits, our studies are restricted to mice, and we do not definitively know whether PNMA2 capsids in humans are responsible for the neurological deficits observed in patients with anti-Ma2 paraneoplastic syndrome. Precisely how PNMA2 capsids trigger the immune response will require further in-depth studies and the development of more chronic models, such as tumor implants, may be required to fully recapitulate human neuropathology and symptoms.

STAR★METHODS

Detailed methods are provided in the online version of this paper and include the following:

SUPPLEMENTAL INFORMATION

Supplemental information can be found online at https://doi.org/10.1016/j.cell.2024.01.009.

ACKNOWLEDGMENTS

We thank Wesley Sundquist, John McCullough, and Ben Schmitz (Department of Biochemistry, University of Utah); Ryan M O'Connell, William Tang, and Warren Voth (Department of Pathology, University of Utah); John E. Greenlee and Noel G. Carlson (Department of Neurology, University of Utah and George E Wahlen VA Medical Center) for helpful discussions and experimental support. We thank Moriel Zelikowsky (Department of Neurobiology, University of Utah) for support and discussions on fear conditioning experiments. We thank the Hind laboratory (Department of Chemical and Biological Engineering, University of Colorado, Boulder) for providing the Luminex machine. We thank all members of the Shepherd lab for technical help and support. The graphic abstract was created with BioRender.com.

S.E. was supported by the Novo Nordisk Foundation (NNF17OC0030788); G.A.H. by NIH T32 CA174648; A.M.W. by NIH R01 NS131660 and the ALS Association; C.F. by NIH R35 GM122550; J.A.G.B. by the Max Planck Society and Medical Research Council (MC_UP_1201/16); J.D.S. by NIH R01 NS115716, the Chan-Zuckerberg Initiative Ben Barres Early Acceleration Award, the Brain Research Foundation Scientific Innovation Award, and the Jon M. Huntsman Presidential Endowed Chair fund.

AUTHOR CONTRIBUTIONS

J.X. performed the biochemistry, electron microscopy, ELISA, RNAscope, immunohistochemistry, mice immunization, and behavior experiments. S.E. conducted the cryo-EM experiments and structure determination. M.S. performed phylogenetic and RNA-seq analysis. M.R. conducted RNAscope, mice immunization, blood collection and helped with behavior experiments. G.A.H. performed the *in vitro* dendritic cell activation and cytokine assays.

I.I. performed mass photometry experiments. J.E. and M.H. generated rat primary cultured neurons. G.S.D., A.L.P., T.L.S., and S.L.C. provided the clinical human samples. J.X., S.E., M.S., G.A.H., M.R., A.M.W., C.F., J.A.G.B., and J.D.S. conceived and designed experiments. J.X. and J.D.S. wrote the manuscript; all authors discussed results and edited the manuscript.

DECLARATION OF INTERESTS

C.F. is a consultant for Tessera Therapeutics, Inc. and HAYA Therapeutics, Inc. J.D.S. is a co-founder of VNV, LLC and holds stock in and is a consultant for Aera Therapeutics, Inc., which licenses intellectual property and patents that include PNMA proteins.

Received: February 24, 2023
Revised: September 20, 2023
Accepted: January 5, 2024
Published: January 31, 2024

REFERENCES

1. Rosenfeld, M.R., Eichen, J.G., Wade, D.F., Posner, J.B., and Dalmau, J. (2001). Molecular and clinical diversity in paraneoplastic immunity to Ma proteins. Ann. Neurol. *50*, 339–348.
2. Dalmau, J., Gultekin, S.H., Voltz, R., Hoard, R., DesChamps, T., Balmaceda, C., Batchelor, T., Gerstner, E., Eichen, J., Frennier, J., et al. (1999). Ma1, a novel neuron- and testis-specific protein, is recognized by the serum of patients with paraneoplastic neurological disorders. Brain *122*, 27–39.
3. Voltz, R., Gultekin, S.H., Rosenfeld, M.R., Gerstner, E., Eichen, J., Posner, J.B., and Dalmau, J. (1999). A Serologic Marker of Paraneoplastic Limbic and Brain-Stem Encephalitis in Patients with Testicular Cancer. N. Engl. J. Med. *340*, 1788–1795.
4. Takaji, M., Komatsu, Y., Watakabe, A., Hashikawa, T., and Yamamori, T. (2009). Paraneoplastic antigen-like 5 gene (PNMA5) is preferentially expressed in the association areas in a primate specific manner. Cereb. Cortex *19*, 2865–2879.
5. Schüller, M., Jenne, D., and Voltz, R. (2005). The human PNMA family: novel neuronal proteins implicated in paraneoplastic neurological disease. J. Neuroimmunol. *169*, 172–176.
6. Hoffmann, L.A., Jarius, S., Pellkofer, H.L., Schueller, M., Krumbholz, M., Koenig, F., Johannis, W., La Fougere, C., Newman, T., Vincent, A., et al. (2008). Anti-Ma and anti-Ta associated paraneoplastic neurological syndromes: 22 newly diagnosed patients and review of previous cases. J. Neurol. Neurosurg. Psychiatry *79*, 767–773.
7. Dalmau, J., Graus, F., Villarejo, A., Posner, J.B., Blumenthal, D., Thiessen, B., Saiz, A., Meneses, P., and Rosenfeld, M.R. (2004). Clinical analysis of anti-Ma2-associated encephalitis. Brain *127*, 1831–1844.
8. Cui, T., Hurtig, M., Elgue, G., Li, S.C., Veronesi, G., Essaghir, A., Demoulin, J.B., Pelosi, G., Alimohammadi, M., Öberg, K., et al. (2010). Paraneoplastic antigen Ma2 autoantibodies as specific blood biomarkers for detection of early recurrence of small intestine neuroendocrine tumors. PLoS One *5*, e16010.
9. Lyons, S., Joyce, R., Moynagh, P., O'Donnell, L., Blazkova, S., and Counihan, T.J. (2020). Autoimmune encephalitis associated with Ma2 antibodies and immune checkpoint inhibitor therapy. Pract. Neurol. *20*, 256–259.
10. Hashimoto, R., Tanabe, E., Otsuka, Y., Yoneda, Y., and Kageyama, Y. (2021). Anti-Ma2-Associated Limbic Encephalitis after Termination of Immune Checkpoint Inhibitor Therapy for Malignant Pleural Mesothelioma. Case Rep. Neurol. *13*, 724–728.
11. Campillos, M., Doerks, T., Shah, P.K., and Bork, P. (2006). Computational characterization of multiple Gag-like human proteins. Trends Genet. *22*, 585–589.
12. Segel, M., Lash, B., Song, J., Ladha, A., Liu, C.C., Jin, X., Mekhedov, S.L., Macrae, R.K., Koonin, E.V., and Zhang, F. (2021). Mammalian retrovirus-like protein PEG10 packages its own mRNA and can be pseudotyped for mRNA delivery. Science *373*, 882–889.
13. Kokošar, J., and Kordiš, D. (2013). Genesis and regulatory wiring of retroelement-derived domesticated genes: a phylogenomic perspective. Mol. Biol. Evol. *30*, 1015–1031.
14. Lynch, C., and Tristem, M. (2003). A co-opted gypsy-type LTR-retrotransposon is conserved in the genomes of humans, sheep, mice, and rats. Curr. Biol. *13*, 1518–1523.
15. Ashley, J., Cordy, B., Lucia, D., Fradkin, L.G., Budnik, V., and Thomson, T. (2018). Retrovirus-like Gag protein Arc1 binds RNA and traffics across synaptic boutons. Cell *172*, 262–274.e11.
16. Pastuzyn, E.D., Day, C.E., Kearns, R.B., Kyrke-Smith, M., Taibi, A.V., McCormick, J., Yoder, N., Belnap, D.M., Erlendsson, S., Morado, D.R., et al. (2018). The neuronal gene arc encodes a repurposed retrotransposon gag protein that mediates intercellular RNA transfer. Cell *172*, 275–288.e18.
17. Erlendsson, S., Morado, D.R., Cullen, H.B., Feschotte, C., Shepherd, J.D., and Briggs, J.A.G. (2020). Structures of virus-like capsids formed by the Drosophila neuronal Arc proteins. Nat. Neurosci. *23*, 172–175.
18. Shepherd, J.D., and Bear, M.F. (2011). New views of Arc, a master regulator of synaptic plasticity. Nat. Neurosci. *14*, 279–284.
19. Abrusán, G., Szilágyi, A., Zhang, Y., and Papp, B. (2013). Turning gold into 'junk': transposable elements utilize central proteins of cellular networks. Nucleic Acids Res. *41*, 3190–3200.
20. Cottee, M.A., Letham, S.C., Young, G.R., Stoye, J.P., and Taylor, I.A. (2020). Structure of Drosophila melanogaster ARC1 reveals a repurposed molecule with characteristics of retroviral Gag. Sci. Adv. *6*, eaay6354.
21. Abed, M., Verschueren, E., Budayeva, H., Liu, P., Kirkpatrick, D.S., Reja, R., Kummerfeld, S.K., Webster, J.D., Gierke, S., Reichelt, M., et al. (2019). The Gag protein PEG10 binds to RNA and regulates trophoblast stem cell lineage specification. PLoS One *14*, e0214110.
22. Pandya, N.J., Wang, C., Costa, V., Lopatta, P., Meier, S., Zampeta, F.I., Punt, A.M., Mientjes, E., Grossen, P., Distler, T., et al. (2021). Secreted retrovirus-like GAG-domain-containing protein PEG10 is regulated by UBE3A and is involved in Angelman syndrome pathophysiology. Cell Rep. Med. *2*, 100360.
23. Zurowska, K., Alam, A., Ganser-Pornillos, B.K., and Pornillos, O. (2022). Structural evidence that MOAP1 and PEG10 are derived from retrovirus/retrotransposon Gag proteins. Proteins *90*, 309–313.
24. Ono, R., Kobayashi, S., Wagatsuma, H., Aisaka, K., Kohda, T., Kaneko-Ishino, T., and Ishino, F. (2001). A retrotransposon-derived gene, PEG10, is a novel imprinted gene located on human chromosome 7q21. Genomics *73*, 232–237.
25. Hantak, M.P., Einstein, J., Kearns, R.B., and Shepherd, J.D. (2021). Intercellular communication in the nervous system goes viral. Trends Neurosci. *44*, 248–259.
26. GTEx Consortium (2013). The genotype-tissue expression (GTEx) project. Nat. Genet. *45*, 580–585.
27. Allen Institute for Brain Science (2017). Allen Brain Atlas: Mouse Brain. https://mouse.brain-map.org/.
28. Hodge, R.D., Bakken, T.E., Miller, J.A., Smith, K.A., Barkan, E.R., Graybuck, L.T., Close, J.L., Long, B., Johansen, N., Penn, O., et al. (2019). Conserved cell types with divergent features in human versus mouse cortex. Nature *573*, 61–68.
29. Zeisel, A., Muñoz-Manchado, A.B., Codeluppi, S., Lönnerberg, P., La Manno, G., Juréus, A., Marques, S., Munguba, H., He, L., Betsholtz, C., et al. (2015). Brain structure. Cell types in the mouse cortex and hippocampus revealed by single-cell RNA-seq. Science *347*, 1138–1142.

30. Shen, E.H., Overly, C.C., and Jones, A.R. (2012). The Allen Human Brain Atlas: comprehensive gene expression mapping of the human brain. Trends Neurosci. *35*, 711–714.

31. Khrameeva, E., Kurochkin, I., Han, D., Guijarro, P., Kanton, S., Santel, M., Qian, Z., Rong, S., Mazin, P., Sabirov, M., et al. (2020). Single-cell-resolution transcriptome map of human, chimpanzee, bonobo, and macaque brains. Genome Res. *30*, 776–789.

32. Dodonova, S.O., Prinz, S., Bilanchone, V., Sandmeyer, S., and Briggs, J.A.G. (2019). Structure of the Ty3/Gypsy retrotransposon capsid and the evolution of retroviruses. Proc. Natl. Acad. Sci. USA *116*, 10048–10057.

33. Tlemsani, C., Pongor, L., Elloumi, F., Girard, L., Huffman, K.E., Roper, N., Varma, S., Luna, A., Rajapakse, V.N., Sebastian, R., et al. (2020). SCLC-CellMiner: a resource for small cell lung cancer cell line genomics and pharmacology based on genomic signatures. Cell Rep. *33*, 108296.

34. Bremmer, F., Bohnenberger, H., Küffer, S., Oellerich, T., Serve, H., Urlaub, H., Strauss, A., Maatoug, Y., Behnes, C.L., Oing, C., et al. (2019). Proteomic comparison of malignant human germ cell tumor cell lines. Dis. Markers *2019*, 8298524.

35. Yufenyuy, E.L., and Aiken, C. (2013). The NTD-CTD intersubunit interface plays a critical role in assembly and stabilization of the HIV-1 capsid. Retrovirology *10*, 29.

36. Bachmann, M.F., and Jennings, G.T. (2010). Vaccine delivery: a matter of size, geometry, kinetics and molecular patterns. Nat. Rev. Immunol. *10*, 787–796.

37. Gause, K.T., Wheatley, A.K., Cui, J., Yan, Y., Kent, S.J., and Caruso, F. (2017). Immunological principles guiding the rational design of particles for vaccine delivery. ACS Nano *11*, 54–68.

38. Bachmann, M.F., Rohrer, U.H., Kündig, T.M., Bürki, K., Hengartner, H., and Zinkernagel, R.M. (1993). The influence of antigen organization on B cell responsiveness. Science *262*, 1448–1451.

39. Jegerlehner, A., Storni, T., Lipowsky, G., Schmid, M., Pumpens, P., and Bachmann, M.F. (2002). Regulation of IgG antibody responses by epitope density and CD21-mediated costimulation. Eur. J. Immunol. *32*, 3305–3314.

40. Murin, C.D., Wilson, I.A., and Ward, A.B. (2019). Antibody responses to viral infections: a structural perspective across three different enveloped viruses. Nat. Microbiol. *4*, 734–747.

41. Arias, C.F., and DuBois, R.M. (2017). The astrovirus capsid: a review. Viruses *9*, 15.

42. Mellman, I., and Steinman, R.M. (2001). Dendritic cells: specialized and regulated antigen processing machines. Cell *106*, 255–258.

43. Lanzavecchia, A., and Sallusto, F. (2001). Regulation of T cell immunity by dendritic cells. Cell *106*, 263–266.

44. Yin, X., Chen, S., and Eisenbarth, S.C. (2021). Dendritic cell regulation of T helper cells. Annu. Rev. Immunol. *39*, 759–790.

45. Park, M.S., Bae, J.H., Jeong, H.B., Kim, J.M., Kwon, O.S., Youn, Y.C., and Ahn, S.W. (2015). Anti-Ma2 antibody encephalitis manifesting as cognitive impairment and psychosis. J. Neuropsychiatry Clin. Neurosci. *27*, e221–e222.

46. Zelikowsky, M., Hersman, S., Chawla, M.K., Barnes, C.A., and Fanselow, M.S. (2014). Neuronal ensembles in amygdala, hippocampus, and prefrontal cortex track differential components of contextual fear. J. Neurosci. *34*, 8462–8466.

47. Mattei, S., Glass, B., Hagen, W.J., Kräusslich, H.G., and Briggs, J.A. (2016). The structure and flexibility of conical HIV-1 capsids determined within intact virions. Science *354*, 1434–1437.

48. Henriques, W.S., Young, J.M., Nemudryi, A., Nemudraia, A., Wiedenheft, B., and Malik, H.S. (2023). The diverse evolutionary histories of domesticated metaviral capsid genes in mammals. Preprint at bioRxiv.

49. Ponpuak, M., Mandell, M.A., Kimura, T., Chauhan, S., Cleyrat, C., and Deretic, V. (2015). Secretory autophagy. Curr. Opin. Cell Biol. *35*, 106–116.

50. Blott, E.J., and Griffiths, G.M. (2002). Secretory lysosomes. Nat. Rev. Mol. Cell Biol. *3*, 122–131.

51. Berns, K.I., and Linden, R.M. (1995). The cryptic life style of adeno-associated virus *17*, 237–245.

52. Pertel, T., Hausmann, S., Morger, D., Züger, S., Guerra, J., Lascano, J., Reinhard, C., Santoni, F.A., Uchil, P.D., Chatel, L., et al. (2011). TRIM5 is an innate immune sensor for the retrovirus capsid lattice. Nature *472*, 361–365.

53. Hubo, M., Trinschek, B., Kryczanowsky, F., Tuettenberg, A., Steinbrink, K., and Jonuleit, H. (2013). Costimulatory molecules on immunogenic versus tolerogenic human dendritic cells. Front. Immunol. *4*, 82.

54. Tam, O.H., Ostrow, L.W., and Gale Hammell, M. (2019). Diseases of the nERVous system: retrotransposon activity in neurodegenerative disease. Mobile DNA *10*, 32.

55. Jansz, N., and Faulkner, G.J. (2021). Endogenous retroviruses in the origins and treatment of cancer. Genome Biol. *22*, 147.

56. Greenlee, J.E., Clawson, S.A., Hill, K.E., Wood, B., Clardy, S.L., Tsunoda, I., Jaskowski, T.D., and Carlson, N.G. (2014). Neuronal uptake of anti-Hu antibody, but not anti-Ri antibody, leads to cell death in brain slice cultures. J. Neuroinflammation *11*, 160.

57. Hughes, E.G., Peng, X., Gleichman, A.J., Lai, M., Zhou, L., Tsou, R., Parsons, T.D., Lynch, D.R., Dalmau, J., and Balice-Gordon, R.J. (2010). Cellular and synaptic mechanisms of anti-NMDA receptor encephalitis. J. Neurosci. *30*, 5866–5875.

58. Graus, F., Delattre, J.Y., Antoine, J.C., Dalmau, J., Giometto, B., Grisold, W., Honnorat, J., Smitt, P.S., Vedeler, Ch., Verschuuren, J.J., et al. (2004). Recommended diagnostic criteria for paraneoplastic neurological syndromes. J. Neurol. Neurosurg. Psychiatry *75*, 1135–1140.

59. Greenlee, J.E., Carlson, N.G., Abbatemarco, J.R., Herdlevær, I., Clardy, S.L., and Vedeler, C.A. (2021). Paraneoplastic and other autoimmune encephalitides: antineuronal antibodies, T lymphocytes, and questions of pathogenesis. Front. Neurol. *12*, 744653.

60. Stewart, S.A., Dykxhoorn, D.M., Palliser, D., Mizuno, H., Yu, E.Y., An, D.S., Sabatini, D.M., Chen, I.S., Hahn, W.C., Sharp, P.A., et al. (2003). Lentivirus-delivered stable gene silencing by RNAi in primary cells. Rna *9*, 493–501.

61. Schindelin, J., Arganda-Carreras, I., Frise, E., Kaynig, V., Longair, M., Pietzsch, T., Preibisch, S., Rueden, C., Saalfeld, S., Schmid, B., et al. (2012). Fiji: an open-source platform for biological-image analysis. Nat. Methods *9*, 676–682.

62. Jumper, J., Evans, R., Pritzel, A., Green, T., Figurnov, M., Ronneberger, O., Tunyasuvunakool, K., Bates, R., Žídek, A., Potapenko, A., et al. (2021). Highly accurate protein structure prediction with AlphaFold. Nature *596*, 583–589.

63. Kimanius, D., Dong, L., Sharov, G., Nakane, T., and Scheres, S.H.W. (2021). New tools for automated cryo-EM single-particle analysis in RELION-4.0. Biochem. J. *478*, 4169–4185.

64. Rohou, A., and Grigorieff, N. (2015). CTFFIND4: Fast and accurate defocus estimation from electron micrographs. J. Struct. Biol. *192*, 216–221.

65. Pettersen, E.F., Goddard, T.D., Huang, C.C., Couch, G.S., Greenblatt, D.M., Meng, E.C., and Ferrin, T.E. (2004). UCSF Chimera—a visualization system for exploratory research and analysis. J. Comput. Chem. *25*, 1605–1612.

66. Emsley, P., and Cowtan, K. (2004). Coot: model-building tools for molecular graphics. Acta Crystallogr. D Biol. Crystallogr. *60*, 2126–2132.

67. Liebschner, D., Afonine, P.V., Baker, M.L., Bunkóczi, G., Chen, V.B., Croll, T.I., Hintze, B., Hung, L.-W., Jain, S., and McCoy, A.J. (2019). Macromolecular structure determination using X-rays, neutrons and electrons: recent developments in Phenix. Acta Crystallogr. D Struct. Biol. *75*, 861–877.

68. Croll, T.I. (2018). ISOLDE: a physically realistic environment for model building into low-resolution electron-density maps. Acta Crystallogr. D Struct. Biol. *74*, 519–530.

69. Shepherd, J.D., Rumbaugh, G., Wu, J., Chowdhury, S., Plath, N., Kuhl, D., Huganir, R.L., and Worley, P.F. (2006). Arc/Arg3.1 mediates homeostatic synaptic scaling of AMPA receptors. Neuron *52*, 475–484.

70. Bepler, T., Kelley, K., Noble, A.J., and Berger, B. (2020). Topaz-Denoise: general deep denoising models for cryoEM and cryoET. Nat. Commun. *11*, 5208.

71. Kucukelbir, A., Sigworth, F.J., and Tagare, H.D. (2014). Quantifying the local resolution of cryo-EM density maps. Nat. Methods *11*, 63–65.

STAR★METHODS

KEY RESOURCES TABLE

REAGENT or RESOURCE	SOURCE	IDENTIFIER
Antibodies		
PNMA2 (rabbit polyclonal, 1:1000 in WB)	Proteintech	Cat# 16445-1-AP; RRID: AB_2167626
PNMA2 (rabbit polyclonal, 1:1000 in WB)	Sigma-Aldrich	Cat# HPA001936; RRID: AB_1079647
Myc (mouse monoclonal, 1:1000 in WB)	Millipore	Cat# 05-724; RRID: AB_309938
Arc (Rabbit polyclonal, 1:1000 in WB)	Synaptic System	Cat# 156 003; RRID:AB_887694
ALIX (rabbit monoclonal, 1:500 in WB)	Gift from Wesley Sundquist lab at University of Utah	N/A
NeuN (guinea pig poloclonal, 1:500 in IHC)	Millipore	Cat# ABN90; RRID: AB_11205592
GFAP (goat Polyclonal, 1:500 in IHC)	Sigma-Aldrich	Cat# SAB2500462; RRID: AB_10603437
IBA-1(goat Polyclonal, 1:500 in IHC)	Novus	Cat# NB 100-1028; RRID: AB_521594
CD3 (rat monoclonal, 1:250 in IHC)	Thermo Fisher Scientific	Cat# 14-0032-82; RRID: AB_467053
CD19 (rat monoclonal, 1:250 in IHC)	Thermo Fisher Scientific	Cat# 14-0193-82; RRID: AB_657650
Goat anti-rabbit IgG HRP (goat polyclonal, 1:5000 in WB)	Jackson ImmunoResearch Labs	Cat# 111-035-003; RRID: AB_2313567
Goat anti-mouse IgG HRP (goat polyclonal, 1:5000 in WB and ELISA)	Jackson ImmunoResearch Labs	Cat# 115-035-003; RRID: AB_10015289
Goat anti-human IgG HRP (goat polyclonal, 1:5000 in ELISA)	Jackson ImmunoResearch Labs	Cat# 109-035-003; RRID: AB_2337577
Alexa Fluor 647-AffiniPure donkey anti-goat IgG (H+L) (donkey polyclonal, 1:1000 in IHC)	Jackson ImmunoResearch Labs	Cat# 705-605-003; RRID: AB_2340436
Alexa Fluor 488-AffiniPure donkey anti-rat IgG (H+L) (donkey polyclonal, 1:1000 in IHC)	Jackson ImmunoResearch Labs	Cat# 712-545-153; RRID: AB_2340684
Alexa Fluor 555 goat anti-rat IgG H&L (goat polyclonal, 1:1000 in IHC)	Abcam	Cat# ab150166
Alexa Fluor 647 goat anti-guinea pig 647 (goat polyclonal, 1:1000 in IHC)	Thermo Fisher Scientific	Cat# A-21450; RRID: AB_2535867
Goat anti-mouse IgG immunogold 6nm	Electron microscopy sciences	Cat# 25124
Goat anti-human IgG immunogold 6nm	Electron microscopy sciences	Cat# 25204
TruStain FcX PLUS anti-mouse CD16/32 (rat monoclonal, 1:50 in FC)	Biolegend	Cat# 156603; RRID: AB_2783137
FITC anti-mouse I-A/I-E (rat monoclonal, 1:100 in FC)	Biolegend	Cat# 107605; RRID: AB_313320
PE/Cy7 anti-mouse CD11c (Armenian Hamster monoclonal, 1:100 in FC)	Biolegend	Cat# 117317; RRID: AB_493569
BV421 anti-mouse CD80 (Armenian Hamster monoclonal, 1:100 in FC)	Biolegend	Cat# 104725; RRID: AB_10900989
BV510 anti-mouse CD86 (Rat monoclonal, 1:100 in FC)	Biolegend	Cat# 105039; RRID: AB_2562370
BV650 anti-mouse CD83 (Rat monoclonal, 1:100 in FC)	Biolegend	Cat# 121515; RRID: AB_11203713
Bacterial and virus strains		
NEB® Stable Competent E. coli (High Efficiency)	New England Biolabs	Cat# C3040H
Rosetta™ 2 Competent Cells	Sigma-Aldrich	Cat# 71402-4
mPNMA2 lentivirus	This paper	N/A

(*Continued on next page*)

Continued

REAGENT or RESOURCE	SOURCE	IDENTIFIER
Biological samples		
Human PNMA2 antibody positive CSF	Mayo Clinic; University of Colorado, Aurora	N/A
Human PNMA2 antibody negative CSF	Antineuronal Antibodies in Autoimmune Neurological Disease biorepository, University of Utah – IRB #00001919	N/A
Chemicals, peptides, and recombinant proteins		
mPNMA2 protein (full length)	This paper	N/A
hPNMA2 protein (full length)	This paper	N/A
Myc-mPNMA2 1-170 peptide	This paper	N/A
Myc-mPNMA2 171-365 peptide	This paper	N/A
Myc-hPNMA2 1-170 peptide	This paper	N/A
Myc-mPNMA2 171-364 peptide	This paper	N/A
Glutathione Sepharose 4B GST-tagged protein purification resin	Cytiva	Cat# 17075601
PreScission Protease	Sigma-Aldrich	Cat# GE27-0843-01
L-Glutathione reduced	Sigma-Aldrich	Cat# G4251
ELISA MaxiSorp plate	Thermo Fisher Scientific	Cat# 468667
ELISA buffer Kit	Thermo Fisher Scientific	Cat# CNB0011
Clarity Western ECL Substrate	Bio-Rad	Cat#1705060
1% Uranyl Acetate Solution	Electron microscopy sciences	Cat# 22400-1
Formvar/Carbon 200 Mesh, Cu	Electron microscopy sciences	Cat# FCF200-Cu
Quantifoil 2/2 Au 2nm C grids	Agar Scientific	Cat# AGS173-8-2CL
qEVoriginal Columns	Izon	Cat# qEVoriginal 35nm
Cytosine β-D-arabinofuranoside	Sigma-Aldrich	Cat# C1768
Poly-L-lysine hydrobromide	Sigma-Aldrich	Cat# P2636
B-27 Supplement (50X), serum free	Thermo Fisher Scientific	Cat# 17504044
BrainPhys Neuronal Medium and SM1 Kit	StemCell Technologies	Cat# 05792
Fetal Bovine Serum	ATCC	Cat# 30-2020
Fetal Bovine Serum	Thermo Fisher Scientific	Cat# 16140071
Neurobasal™ Medium	Thermo Fisher Scientific	Cat# 21103049
DMEM, high glucose	Thermo Fisher Scientific	Cat# 11965118
DMEM, no phenol red	Thermo Fisher Scientific	Cat# 31053028
RPMI 1640 Medium	Thermo Fisher Scientific	Cat# A1049101
Propidium Iodide (1:100 in FC)	Biolegend	Cat# 421301
Murine GM-CSF (20ng/mL for BMDC generation)	Peprotech	Cat# 315-03
LPS (1ng/mL for BMDC stimulation)	Invivogen	Cat# tlrl-3pelps
Red Blood Cell Lysing Buffer Hybri-Max	Millipore Sigma	Cat# R7757
Critical commercial assays		
ProcartaPlex™ Mouse Cytokine & Chemokine Convenience Panel 1, 26plex	Invitrogen	Cat# EPXR260-26088-901
PNMA2 RNAscope	ACD Bio	Cat# 1045221-C1
CyQUANT™ LDH Cytotoxicity Assay	Invitrogen	Cat# C20300
Deposited data		
mPNMA2 full capsid monomer structure	This paper	EMD-19024; PDB 8RB3
mPNMA2 capsid local reconstruction fivefold structure	This paper	EMD-19025; PDB 8RB4
mPNMA2 capsid local reconstruction threefold structure	This paper	EMD-19026; PDB 8RB5

(*Continued on next page*)

Continued

REAGENT or RESOURCE	SOURCE	IDENTIFIER
mPNMA2 capsid local reconstruction twofold structure	This paper	EMD-19027; PDB 8RB7
Bulk tissue gene expression for PNMA2	The genotype-tissue expression (GTEx) project	gtexportal.org/home/gene/ENSG00000240694
Single-cell RNA-seq data of mouse cortex and hippocampus	Gene Expression Omnibus	GEO: https://www.ncbi.nlm.nih.gov/geo/query/acc.cgi?acc=GSE60361
Single-nucleus RAN-seq data of the middle temporal gyrus of human cortex	Allen Brain Altas	https://celltypes.brain-map.org/
Single-cell-resolution transcriptome map of human, chimpanzee, bonobo, and macaque brains	Gene Expression Omnibus	GEO: https://www.ncbi.nlm.nih.gov/geo/query/acc.cgi?acc=GSE127898
Gene expression profile in primary cancer samples of patients	Cancer Genome Atlas (TCGA) consortium	https://docs.gdc.cancer.gov/Encyclopedia/pages/Annotations_TCGA/
Experimental models: Cell lines		
Human: HEK293T	ATCC	Cat# CRL-3216; RRID: CVCL_0063
Human: NTERA-2	ATCC	Cat# CRL-1973; RRID: CVCL_3407
Human: NCI-H378	ATCC	Cat# CRL-5808
Mouse: MC-38	Gift from Ryan M O'Connell lab at the University of Utah	N/A
Cultured rat primary cortical neurons (Sprague-Dawley)	This paper	N/A
Cultured rat primary hippocampal neurons (Sprague-Dawley)	This paper	N/A
Cultured mouse bone marrow-derived dendritic cells (C57BL/6)	This paper	N/A
Experimental models: Organisms/strains		
Rat Sprague-Dawley	Charles River	RRID: RGD_734476
Mouse C57BL/6	University of Utah	RRID: IMSR_JAX:000664
Recombinant DNA		
pGEX-6p1-mPNMA2	This paper	N/A
pGEX-6p1-hPNMA2	This paper	N/A
pGEX-6p1-mPNMA2 1-170	This paper	N/A
pGEX-6p1-mPNMA2 171-365	This paper	N/A
pGEX-6p1-hPNMA2 1_170	This paper	N/A
pGEX-6p1-hPNMA2 171-364	This paper	N/A
pGEX-6p1-mPNMA2 Y162A	This paper	N/A
pGEX-6p1-mPNMA2 L270QL325Q	This paper	N/A
PRK5-myc-mPNMA2	This paper	N/A
pLVX-myc-mPNMA2	This paper	N/A
PLVX-mPNMA2	This paper	N/A
PLVX-mPNMA2 Y162A	This paper	N/A
pLVX-mPNMA2 L270QL325Q	This paper	N/A
pspAX2	Trono Lab (unpublished data)	RRID: Addgene_12260
VSV-G	Stewart et al.[60]	RRID: Addgene_8454
Software and algorithms		
Graphpad Prism 9	Graphpad	http://graphpad.com/; RRID: SCR_000306
ImageJ/Fiji	Schindelin et al.[61]	https://fiji.sc/; RRID: SCR_002285
SnapGene	SnapGene	http://www.snapgene.com/; RRID: SCR_015052
Adobe illustrator 2024	Adobe Systems Incorporated	RRID:SCR_ 010279

(*Continued on next page*)

Continued

REAGENT or RESOURCE	SOURCE	IDENTIFIER
AlphaFold2	Jumper et al.[62]	https://alphafold.ebi.ac.uk/; RRID: SCR_023662
EndNote 21	Endnote	http://endnote.com; RRID: SCR_014001
RELION4	Kimanius et al.[63]	https://relion.readthedocs.io/en/release-4.0/
CTFFIND4	Rohou and Grigorieff[64]	https://github.com/leschzinerlab/myami-3.2-freeHand/blob/master/bin/ctffind4.py
Chimera/ChimeraX	Pettersen et al.[65]	https://www.cgl.ucsf.edu/chimera/
Coot	Emsley and Cowtan[66]	https://www2.mrc-lmb.cam.ac.uk/personal/pemsley/coot/
Phenix	Liebschner et al.[67]	https://phenix-online.org/
ISOLDE	Croll[68]	https://tristanic.github.io/isolde/
PNMA2 phylogenetic analysis and RNA-seq analysis code	This paper	https://doi.org/10.5281/zenodo.10563569
Flowjo	Treestar	https://www.flowjo.com/

RESOURCE AVAILABILITY

Lead contact

Further information and requests for resources or reagents are available from the lead contact, Dr. Jason Shepherd (Jason.Shepherd@neuro.utah.edu).

Materials availability

Materials used in this study will be provided upon request and available upon publication.

Data and code availability

- RNA-seq data used in this study can be found at the following publicly available datasets: https://gtexportal.org/home/gene/ENSG00000240694, https://www.ncbi.nlm.nih.gov/geo/, https://celltypes.brain-map.org/, https://docs.gdc.cancer.gov/Encyclopedia/pages/Annotations_TCGA/
- All statistical and plotting details, including the statistical tests, used, and precision measures for RNA-seq data analysis can be found on a publicly available repository at https://doi.org/10.5281/zenodo.10563569
- Cryo-EM data have been deposited in the Electron Microscopy Data Bank under accession codes EMD-19024, EMD-19025, EMD-19026, and EMD-19027. Corresponding molecular model data have been deposited in the Protein Data Bank under accession codes 8RB3, 8RB4, 8RB5, and 8RB7. Deposited structures and models are summarized in Table S1, and all data are publicly available as of the date of publication.
- Any additional information required to reanalyze the data reported in this paper is available from the lead contact upon request.

EXPERIMENTAL MODEL AND STUDY PARTICIPANT DETAILS

C57BL/6 Mice

Mice were housed in breeding pairs or obtained from Jackson Laboratory as age-matched littermates, or group-housed with littermates of the same sex after weaning (2-5 mice/cage), on a 12:12 h day:night cycle, with food and water provided *ad libitum*. All animal experiments were approved by the Institutional Animal Care and Use Committee of the University of Utah (IACUC protocol #22-02008).

Sprague-Dawley Rats

Female pregnant rats were purchased from Charles River Laboratories (Wilmington, MA). Rats were housed on a 12:12 h day: night cycle, with food and water provided *ad libitum*. Hippocampal and cortical primary neuron cultures were prepared from E18 embryos. All animal experiments were approved by the Institutional Animal Care and Use Committee of the University of Utah.

Human Patients

Paraneoplastic patient information

Patient 1 - PNMA2 (Ma2) antibody positive in CSF. 27-year-old previously healthy male presented with a 2-month history of lethargy and decreased libido. Neurological examination demonstrated normal cognition, with mild dysarthria, bilateral ptosis, slowing of

upward saccades, and decreased arm swing. Screening blood work confirmed low testosterone, follicular stimulating hormone, and luteinizing hormone. Brain MRI disclosed an enhancing mass in the tectal region with dilation of the ventricles. Cerebrospinal fluid analyses (CSF) showed pleocytosis (13 cells per mm3; reference <6 cells per mm3) with lymphocytic predominance, elevated protein (58 mg/dL; reference 15-45 mg/dL), and normal glucose. There were no unique oligoclonal bands. CSF infectious studies were negative including herpes simplex virus polymerase chain reaction. CSF cytology and cytometry were negative for malignant cells. No disease-associated autoantibodies were detected on serum or CSF screening (Mayo Clinical Laboratories, ''autoimmune encephalitis panel'', and anti-aquaporin4 antibodies). Stereotactic-guided tectal biopsy was performed, with pathology confirming a lymphoplasmacytic inflammatory process. Over the ensuing two months, the patient complained of increasing fatigue and lethargy, with double vision attributed to vertical gaze restriction. Repeat neuroimaging showed mild interval improvement in the tectal mass, with normal-sized ventricles, with emergence of bilateral T2-FLAIR signal within the temporal lobes. Atypical paraneoplastic causes were considered, and body imaging completed. Body CT demonstrated numerous sub centimeter nonspecific nodes in the abdomen and pelvis. Testicular ultrasound confirmed bilateral testicular microlithiasis. A diagnosis of ma1/ma2 autoimmune encephalitis was considered; ma2 autoantibodies were confirmed through testing of CSF and serum via Athena Diagnostics. Bilateral orchiectomy was performed given concern of disease-associated tumor. Histopathology was notable for dystrophic calcifications and fibrosis, suggestive of a burnt-out germ cell tumor. High-dose intravenous steroids were provided, with a corresponding brief improvement in alertness and temporal lobe T2-hyperintensities. Long-term follow-up was complicated by treatment-refractory temporal lobe seizures, necessitating escalation of immunotherapy, including monthly intravenous cyclophosphamide. Severe fatigue, lethargy, double vision, and vertical gaze palsy persisted.

Patient 2 - PNMA1 (Ma1) and PNMA2 (Ma2) antibody positive in CSF. 54-year-old female with history of renal cell carcinoma status post-resection presented with a 6-month history of progressive diplopia, gaze paresis, abnormal gait with falls, increasing confusion, and new-onset seizures. On exam, the right eye was deviated downward, adduction was impaired in the left eye, and gait was wide-based and apractic. Brain MRI was markedly abnormal, with symmetric subcortical T2-hyperintensities involving the medial temporal lobes, parietooccipital cortices and medial thalami, concerning for posterior reversible encephalopathy syndrome versus neuroinflammation. CSF analyses disclosed 5 white blood cells (per mm^3), normal glucose, and protein, with 9 CSF-specific oligoclonal bands. Noting the history of renal cancer, body imaging was performed revealing mediastinal and bilateral hilar lymphadenopathy, with bilateral pulmonary nodules and masses, and a left adrenal mass. Lymph nodes were FDG-avid on follow-up PET scan. Mediastinal biopsy confirmed metastatic renal carcinoma. Paraneoplastic panel (Mayo Clinic Laboratories) including Ma1/Ma2 testing (Athena Diagnostics) identified Ma1/Ma2 antibodies in blood and CSF. High dose IV methylprednisone and plasmapheresis (5 exchanges) were provided for treatment of Ma1/Ma2 paraneoplastic encephalitis without improvement. The patient developed a diencephalic syndrome with ophthalmoparesis (near plegia) with "sunsetting eyes", progressive encephalopathy, and cortical blindness. Planned treatment of her underlying malignancy was limited by the development of bilateral pulmonary emboli requiring systemic anticoagulation, and a general decline in physical health. The patient died of complications of her illness.

Patient 3 - PNMA1 (Ma1) and PNMA2 (Ma2) antibody positive in CSF. 66-year-old male with a history of chronic tobacco use presented with two months of worsening balance, diplopia, and confusion. He had no prior medical conditions. Neurological exam revealed short-term memory deficits, a poor fund of knowledge, ataxia, opsoclonus, restricted upgaze, restriction of right eye abduction, and a right extensor toe response. Brain MRI revealed an encephalitis involving the brainstem, mesial temporal lobes, and basal ganglia. CSF analysis showed a pleocytosis of 75 nucleated cells per mm^3 (reference < 6 nucleated cells per mm^3) with a lymphocytic predominance, elevated protein of 75 mg/dL (reference 15–45 mg/dL), and normal glucose. Five CSF-specific oligoclonal bands were present. *PNMA1 (Ma1) and PNMA (Ma2)* were positive (titer > 1:32, Athena Diagnostics). Low positive Anti-NMDA-R antibody was detectable only on a neat, undiluted cell-based assay (Mayo Clinical Laboratories), and serum studies demonstrated low positive anti-GAD65 antibodies at a titer present in up to 8% of the normal population and not generally consistent with symptoms or associated neurologic disease (0.12 nmol/L, reference $\leq$0.02), with the rest of the serum autoimmune encephalopathy evaluation otherwise negative (Mayo Clinical Laboratories). CSF infectious studies were negative including herpes simplex virus polymerase chain reaction. CSF cytology and cytometry were negative for malignant cells. Malignancy screening included a negative testicular ultrasound and a computed tomography (CT) of the chest that demonstrated extensive pulmonary fibrosis, several prominent mediastinal lymph nodes, and multiple segmental pulmonary emboli. A body positron emission tomography CT demonstrated FDG uptake in a right hilar lymph node in addition to a subpleural, sub-centimeter pulmonary nodule in the left upper lobe, but a progressive deterioration of his respiratory status prevented full investigation.

Control/non-paraneoplastic patient information

Patient CSF samples were obtained from the Antineuronal Antibodies in Autoimmune Neurological Disease biorepository, University of Utah – IRB #00001919.

Control Patient 1

60-year-old male with 2 years of progressive spasticity (bilateral lower extremities, progressed to left upper extremity). Neurologic exam notable initially for spasticity and upper motor neuron signs, but no lower motor neuron signs. Initial EMG with no abnormal spontaneous activity and MRI brain, C-, T- spine unremarkable. CK mildly elevated at 304. CSF with 2 WBC (ref 0–5), protein 52 (ref 14–45), glucose 61 (ref 50–80), OCB negative, <0.0 IgG synthesis rate. Autoimmune encephalitis panel (Mayo Clinic Laboratories) evaluation of serum and CSF with no informative autoantibodies detected. Glycine receptor antibody also negative in serum

(not tested in CSF). Washington University in St. Louis neuromuscular antibody panel on serum also unremarkable. Ultimately progressed, and EMG findings with upper and lower motor neuron findings; diagnosed with amyotrophic lateral sclerosis.

Control Patient 2

54-year-old male followed for postherpetic neuralgia. CAF with WBC 0, protein 38, glucose 65, OCB 0, <0.0 IgG synthesis rate. CSF culture negative, HSV1/2 Ab screen IgG <0.34, HSV Type 1 Ab IgG 0.0, HSV 1 and or 2 Abs IgM 0.19, VZV IgG <10, VZV IgM 0.02, VZV PCR not detected, CMV IgM <8, HSV 6 Ab IgM by IFA <1:20. Note- all these results are within normal limits. No send out antibody testing done because no concern for immune-mediated process.

Control Patient 3

58-year-old female with diffuse paresthesia and pain, diagnosed with small fiber neuropathy, pernicious anemia and positive GAD65 antibody (without neurologic manifestations). CSF WBC 5, protein 37, glucose 53, OCB negative (note: matched bands in serum and CSF), IgG synthesis rate <0.0, Mayo Paraneoplastic Autoantibody Evaluation from CSF positive for GAD65 Ab assay 0.04 nmol/L (ref 0.02), negative for AGNA1, Amphiphysin Ab, ANNA1, ANNA2, ANNA3, CRMP5 IgG, PCA1, PCA2, PCA-Tr. Mayo Autoimmune dysautonomia eval (serum) with AChR Ganglionic Neuronal Ab 0.03 nmol/L (ref <0.02), GAD65 Ab 20.1 nmol/L (ref <0.02), negative for ANNA1, Striational Ab, N-type Calcium Channel, Ach Receptor binding Ab, Neuronal VGKC Ab, P/Q Type Calcium channel. Intrinsic factor blocking antibody positive. GAD65 Ab at ARUP >250 IU/mL.

HEK 293T Cells

HEK 293T cells (#CRL-11268) were purchased from ATCC. Cells were cultured at 37°C with 5% CO2 in media including DMEM (Thermo Fisher Scientific, Waltham, MA), 5% fetal bovine serum (Thermo Fisher Scientific, Waltham, MA) and 1% penicillin/streptomycin (Thermo Fisher Scientific, Waltham, MA). Cell cultures were passaged at 70% confluency.

NCI-H378 Cells

NCI-H378 cells (#CRL-5808) were purchased from ATCC. Cells were cultured at 37°C with 5% CO2 in media including RPMI-1640 (ATCC, Manassas, VA), 5% fetal bovine serum (ATCC, Manassas, VA), and 1% penicillin/streptomycin (Thermo Fisher Scientific, Waltham, MA).

NTERA-2 Cells

NTERA-2 cells (#CRL-1973) were purchased from ATCC. Cells were cultured at 37°C with 5% CO2 in media including DMEM (Thermo Fisher Scientific, Waltham, MA), 5% fetal bovine serum (ATCC, Manassas, VA) and 1% penicillin/streptomycin (Thermo Fisher Scientific, Waltham, MA). Cell cultures were passaged at 90% confluency. Lipofectamine 3000 transfection reagent (Thermo Fisher Scientific, Waltham, MA) was used for transfecting myc-mPNMA2 plasmid into NETRA cell culture.

MC-38 Cells

MC-38 cells were obtained from Ryan M O'Connell lab at the University of Utah. Cells were cultured at 37°C with 5% CO2 in media including DMEM (Thermo Fisher Scientific, Waltham, MA), 5% fetal bovine serum (Thermo Fisher Scientific, Waltham, MA) and 1% penicillin/streptomycin (Thermo Fisher Scientific, Waltham, MA). Cell cultures were passaged at 70% confluency.

Bone Marrow Dendritic Cell (BMDC) Culture

To generate BMDC, bone marrow was harvested from the femurs and tibias of 6–10-week-old WT C57BL/6 mice, filtered through a 40μM strainer (Fisher Scientific, Hampton, NH), and treated with Red Blood Cell Lysis Buffer (Hybrimax, Sigma Aldrich, St. Louis, MO) according to manufacturer's recommendations. Following RBC lysis, cells were resuspended in BMDC media containing RPMI 1640 (Corning, NY), 10% Heat Inactivated FBS (Sigma, St. Louis, MO), 1% L-glutamine (R&D Systems, Minneapolis, MN), 1% P/S (Gibco, Waltham, MA), 1% 1M HEPES (Sigma, St. Louis, MO), 50μM 2-mercaptoethanol (Sigma, St. Louis, MO), and 20ng/mL murine GM-CSF (Peprotech, Cranbury, NJ) at a concentration of 0.5e6 cells/mL and plated in 24-well plates for cell culture. Cells were incubated at 37 degrees C with 5% CO_2. Media was changed every 2-3 days

Primary cultured rat cortical/hippocampal neurons

Primary neuron cultures were prepared from male and female E18 rat (Sprague-Dawley) cortex and hippocampus as previously described.[69] Tissue was dissociated in DNase (0.01%; Sigma-Aldrich, St. Louis, MO) and papain (0.067%; Worthington Biochemicals, Lakewood, NJ), and then triturated with a fire-polished glass pipette to obtain a single-cell suspension. Cells were pelleted at 500xg for 4 min, the supernatant removed, and cells resuspended and counted with a TC-20 cell counter (Bio-Rad, Hercules, CA). Neurons were plated on glass coverslips (Carolina Biological Supply, Burlington, NC) coated with poly-l-lysine (0.2 mg/mL: Sigma-Aldrich, St. Louis, MO) in 12-well plates (Greiner Bio-One, Monroe, NC) at 90,000 cells/mL, or in 10-cm plastic dishes at 800,000 cells/mL. Neurons were initially plated in Neurobasal media containing 5% serum, 2% GlutaMAX, 2% B-27, and 1% penicillin/streptomycin (Thermo Fisher Scientific, Waltham, MA) in a 37°C incubator with 5% CO2. On DIV4, neurons were fed via half media exchange with astrocyte-conditioned BrainPhys™ Neuronal Medium (Stemcell Technologies, Vancouver, Canada) containing 1% serum (Thermo Fisher Scientific, Waltham, MA), 0.25% L-Glutamine (Thermo Fisher Scientific, Waltham, MA), 1% penicillin/streptomycin (Thermo Fisher Scientific, Waltham, MA), 2% SM1 (Stemcell Technologies, Vancouver, Canada), and 5 μM cytosine

β-d-arabinofuranoside (AraC) (Sigma-Aldrich, St. Louis, MO). Half media exchange of astrocyte-conditioned media was conducted every three days thereafter.

METHOD DETAILS

Plasmids

The coding sequence (CDS) of mPNMA2, hPNMA2, myc-mPNMA2 1-170aa, myc-mPNMA2 171-365aa, myc-hPNMA2 1-170aa, and myc-hPNMA2 171-364aa, mPNMA2 Y162A, mPNMA2 L270QL325Q were synthesized by Integrated DNA Technologies (Coralville, IA). These fragments were digested by *BamHI* and *XhoI* restriction enzymes (New England BioLabs, Ipswich, MA), and ligated into pGEX-6p1 vector for protein expression and purification. The mPNMA2 CDS was amplified by PCR, digested by *SalI* and *NotI*, and cloned into the PRK5-myc vector. Similarly, pLVX-myc-mPNMA2, pLVX-mPNMA2, pLVX-mPNMA2 L270Q/L325Q, and pLVX-mPNMA2 Y162A were constructed by PCR amplification of mPNMA2 WT and L270QL325Q CDS, *BamHI* and *XhoI* digestion, and ligation into pLVX backbone between *BamHI* and *XhoI* sites. All ligation products were transformed into NEB Stable Competent E. coli (High Efficiency) (New England Biolabs, Ipswich, MA). Individual colonies were inoculated to isolate plasmids and screen for correct constructs by sequencing.

Protein Purification

Bacterial protein expression plasmids were transformed into *E. coli* Rosetta2 strain (Novagen, Gibbstown, NJ) and the protein was expressed in ZY autoinduction media. *E. coli* were grown to 0.6-0.8 of OD600 at 37°C 150rpm, then switched to 19°C for 16-20h shaking. Afterwards, bacteria were pelleted down at 5000g for 15min at 4°C, resuspended in lysis buffer (500mM NaCl, 50mM Tris, 5% glycerol, 1mM DTT, complete Protease Inhibitor Cocktail, pH 8.0). The resuspended bacteria were frozen by liquid nitrogen and then thawed. The thawed lysates were sonicated and centrifuged at 21,000g for 45mins at 4°C. The supernatant was filtered through 0.45μm filters and incubated with Sepharose 4B beads (Cytiva, Marlborough, MA) overnight at 4°C. GST-tagged proteins were eluted from Sepharose beads by incubating with L-reduced glutathione (20mM, pH 8.0) and exchanged to cleavage buffer (50mM Tris, 150mM NaCl, 1mM DTT, 1mM EDTA, pH 7.2) using a Vivaspin column (Cytiva, Marlborough, MA). The cleavage of GST was performed by PreScission Protease (Cytiva, Marlborough, MA) overnight at 4°C. The cleaved PNMA2 protein was run through a HiLoad 16/600 Superdex 200 pg (Cytiva, Marlborough, MA) size-exclusion column in the capsid assembly buffer (500mM phosphate, 50mM Tris, 0.5mM EDTA, pH 7.5) to further purify PNMA2 and facilitate capsid formation. For protein purified for mice immunization, Triton X-114 was used to wash GST-tagged protein bound to Sepharose beads to remove endotoxin.

Negative-staining Electron Microscopy

Copper 200-mesh grids coated with formvar and carbon (Electron Microscopy Sciences, Hatfield, PA) were discharged for 30s in a vacuum chamber. Grids were incubated with 3.5μL purified protein (0.5mg/mL) for 45s and excess sample was wicked away. Grids were then immediately washed twice with 30uL water for 5 s and once with 15μL 1% uranyl acetate (UA) for 5s. Excess UA was wicked away and the grids were stained with 15μL 1% UA for 30s. Excess UA was wicked away and grids were air-dried. The grids were imaged using a FEI Tecnai T12 Transmission Electron Microscope operated at 120kV.

Cryo-EM

4 μL of mPNMA2 capsids at a concentration of ~1 mg/ml were applied to glow discharged QUANTIFOIL 2/2 Au continuous carbon grids. The sample was blotted and plunge-frozen in liquid ethane using a Vitrobot Mark IV. CryoEM images were acquired on a 300 keV FEI Titan Krios microscope with X-FEG emitter equipped with a Falcon III detector operated in counting mode. mPNMA2 datasets were collected using EPU (ThermoFisher) at a nominal magnification of 96000x with a calibrated pixel sizes of 0.832 Å. Micrographs were recorded as movies divided into 75 frames with a final accumulated dose of 40 e/Å^2. Defocus values ranged from −0.5 to −2.5 μm.

CryoEM Image Processing

mPMNA2 image processing and reconstructions are summarized in Figure S3 and Table S1. Acquired movies were aligned using 5x5 patches, averaged and dose-weighted using RELION4.[63] Contrast transfer function (CTF) parameters were estimated using CTFFIND4.[64] Particles were automatically picked using a retrained topaz model.[70] Boxsize used for extraction was 512x512 pixels. Extracted particles were subjected to several rounds of 2D classification to remove false picks and junk particles. 2D classes showed views characteristic for icosahedral symmetry, and icosahedral symmetry (I) was applied for initial model generation and throughout subsequent 3D classification and refinement. Finally, we performed per-particle CTF estimation, Bayesian polishing and Ewald sphere correction. The effective resolutions of the cryoEM density maps were estimated by Fourier shell correlation (FSC = 0.143).

To further improve the resolution, we performed symmetry expansion as implemented in RELION4, to calculate the positions and orientations for each of the asymmetric units centered either at the five, three or two-fold symmetric axes. We extracted individual capsomeres using box sizes of 220x220 pixels. We performed 3D classification without alignment to remove bad views and to select classes for subsequent refinement. For all maps, local resolutions were calculated using ResMap[71] and maps were locally sharpened using Phenix.[67]

Structure Model Building

For model building we used Alphafold2[62] to generate an initial model (Figure S4I). After initial rough fitting using chimera,[65] we went through several rounds of manual and auto-refinement in coot, Phenix, and ISOLDE.[66,68] Model statistics are shown in Table S1.

Mass Photometry

Mass photometry was performed on a Refeyn TwoMP mass photometer. Protein stocks were brought to room temperature and diluted with stock buffer (500mM Na2HPO4, 50mM Tris, 10% glycerol, pH 7.5) to a concentration of 100nM. A 20 μl droplet of each sample dilution was placed on top of a clean chambered coverslip mounted on the oil objective of the instrument. Following autofocus stabilization, a one-minute movie was recorded using the Aquire-MP (Refeyn) software. A protein standard containing equimolar amounts of four proteins (conalbumin, aldolase, ferritin, and thyroglobulin) with a molecular mass ranging from 75 to 669 kDa was also measured and used for calibration. Movies were converted to mass using a contrast-to-mass calibration and analyzed using the Discover-MP software (Refeyn).

HEK 293T Transfection

10 cm dish transfection: 9μg of plasmids and 25μL of 1μg/μL Polyethylenimine (Polysciences, Warrington, PA) were mixed in 1mL Opti-MEM (Thermo Fisher Scientific, Waltham, MA) and incubated at room temperature for 20 minutes. This mixture was added to 60% confluent cell culture in transfection media (DMEM+10% FBS) and incubated overnight.

LDH Cytotoxicity Assay

The amount of LDH in the cell lysates and media was measured using CyQUANT LDH Cytotoxicity Assay kit (Thermo Fisher Scientific, Waltham, MA). The percentage of cell death was calculated by the total amount of LDH in the media divided by that in the cell lysates.

Lentivirus Production and Transduction

HEK293 cells in a 10 cm dish were transfected with VSVG1.0, psPAX2, and pLVX- mPNMA2 overnight. Transfection media was changed to regular culture media (DMEM+10% FBS+ 1% penicillin/streptomycin). The media was collected 24 hours later and centrifuged at 1,000g for 10min. 20mM HEPES was added to the supernatant and centrifuged at 5,000g overnight. Lentivirus particles were pelleted and resuspended in 400 μL PBS. MC-38 cells in a 10 cm dish were transduced with 200 μL lentivirus particles at for 2 days and then selected with 10μg/mL puromycin to make a stable cell line overexpressing mPNMA2.

Protein Injections in Mice

10–12-week-old mice (C57BL/6) were injected intraperitoneally with vehicle (200μl of capsid assembly buffer), 5μg of mPNMA2 capsids, or 5μg of mPNMA2 L270QL325Q capsid mutant on day 0. The injected proteins were not mixed with any adjuvant. Blood was collected on day 21 via the tail vein. A second injection of 5μg of mPNMA2 capsids, L270QL325Q capsid mutant, and vehicle were performed on day 21 and blood was collected on day 42. Endotoxin was removed from the purified protein by Triton X-114 wash. Preparations were checked for the presence of capsids via negative stain EM, prior to injection.

Serum Processing

Blood was coagulated at 4°C overnight and serum was harvested by centrifuging twice at 2,000g for 10 min to collect the supernatant.

Extracellular Vesicle and Capsid Purification from Culture Media

For HEK 293T cells, full media change was performed 12 hours after transfection and then collected 24 hours later. For neuronal culture, full media change was performed at DIV15 (2 days after lentivirus transduction) and then collected 24 hours later. Collected media was centrifuged at 2,000g for 10min and then 20,000g for 20min. The supernatant of the collected media was concentrated into 0.5mL using Vivaspin 100 KDa columns. Concentrated media was loaded onto IZON mini-size exclusion columns (IZON Sciences, Christchurch, New Zealand). The first 3mL run through the column was collected as the void fraction. Then, every 0.5mL was collected for a total of 11 fractions, labeled as fraction 1 to 11.

Proteinase K Protection Assay

Cultured media was processed using IZON columns as above and treated with three different conditions: 1. 20μL sample + 7μL H2O or 2. 20μL sample + 6μL H2O + 1μL proteinase K (200μg/mL) (New England BioLabs, Ipswich, MA) or 3. 20μL particle sample + 3μL H2O + 3μL 10% Triton X-100 + 1μL proteinase K (200μg/mL). Media was incubated at room temperature for 10 min. Then, 3μL of 10mM PMSF was added and incubated for 10min at room temperature. Finally, samples were mixed with Laemmle buffer (40% glycerol, 250 mM Tris, 4% SDS, 50 mM DTT, pH 6.8) and boiled at 95°C for 5 min.

Western Blot and Antibodies

Samples were mixed with 4x Laemmle buffer and incubated at 95°C for 5 mins. Proteins were loaded and separated by 10% or 12% SDS-PAGE gel, followed by wet transfer to a nitrocellulose membrane (GE Healthcare, Chicago, IL). Total protein was stained and destained by Pierce Reversible Protein Stain Kit (Thermo Fisher Scientific, Waltham, MA). The membrane was blocked by 5% milk in

TBS for 1h at room temperature. Primary antibodies were diluted in 1% milk in TBS and incubated with the membrane at 4°C overnight. Primary antibodies include: anti-myc (05-724, Sigma-Aldrich, St. Louis, MO; 1:1000), anti-PNMA2 (16445-1-AP, Proteintech, Rosemont, Illinois; 1:1000; HPA001936, Sigma-Aldrich, St. Louis, MO, 1:1000), anti-Alix (customized antibody from Wesley Sundquist's lab; 1:500), mice sera (1:1000). The membrane was washed by TBS and then incubated with secondary antibodies (anti-mouse IgG, anti-rabbit IgG, anti-human IgG, Jackson Laboratory, Bar Harbor, ME; 1:5000) diluted by 1% milk in TBS for 1h at room temperature. Afterwards, the membrane was washed with TBS for three times. Bound antibodies were detected by Clarity™ Western ECL Substrate (Bio-Rad, Hercules, CA) and imaged using an Amersham ImageQuant™ 800 Western blot imaging systems (Cytiva, Marlborough, MA). Images were analyzed and quantified using ImageJ.

RNA-Scope

Brian tissues obtained from 2-month-old mice and primary hippocampal neuronal cultures (DIV15) were used for RNAscope. RNAscope multiplex fluorescent v2 assay kit and the probe were purchased from Advanced Cell Diagnostics (Hayward, CA). The probe was tagged to opal 570 dye from Akoya Biosciences (Marlborough, MA).

Immunohistochemistry and Antibodies

Brain tissue sections (40μm thick) were blocked by blocking buffer at room temperature for 2h. Primary antibodies in blocking buffer (5% normal donkey/goat serum, 2% fish gelatin, 0.1% Triton X-100, 0.05% sodium azide in PBS) were incubated with brain tissue overnight at room temperature. Primary antibodies include: anti-GFAP (SAB2500462, Sigma-Aldrich, St. Louis, MO, 1:1000), anti-IBA-1 (NB100-1028, Centennial CO, 1:500), anti-NeuN (ABN90, MilliporeSigma, Burlington, MA,1:1000), anti-CD3 (14-0032-82, Thermo Fisher Scientific, Waltham, MA, 1:250), anti-CD19(14-0193-82, Thermo Fisher Scientific, Waltham, MA, 1:250). Afterward, the tissue was washed with wash buffer (2% fish gelatin, 0.1% Triton X-100, 0.05% sodium azide in PBS) 3 times across 24h at room temperature. Fluorescent secondary antibodies (Jackson ImmunoResearch Laboratories, West Grove, PA, 1:1000) were then incubated with tissue at room temperature overnight and washed 3 times across 24h at room temperature. Tissues were finally mounted with Fluoromount-G (DAPI) (Thermo Fisher Scientific, Waltham, MA).

Confocal Imaging

Coverslips were imaged using a 10x objective for brain tissues and 60x oil objective for cultured neurons on a Nikon C2+ inverted confocal system (Tokyo, Japan). The images were analyzed using ImageJ software (National Institutes of Health, Bethesda, MD).

Iodixanol Gradient Ultracentrifugation

An Iodixanol gradient was made with 2mL 15% (1M NaCl), 3mL 30%, 3mL 40% and 3mL 50% OptiPrep™ iodixanol (Alere Technologies AS, Oslo, Norway). 500μL of the sample was added to the top of the gradient and centrifuged at 100,000g for 48 hours. After ultracentrifugation, sequential 1mL collections were made from the top of the gradient and labeled as fractions 1 to 12.

Immunogold EM

Copper 200-mesh grids coated with formvar and carbon (Electron Microscopy Sciences, Hatfield, PA) were discharged for 30s in a vacuum chamber. PNMA2 purified protein (0.1mg/mL, 3.5μL) was loaded onto the grid and incubated for 45s. Grids were washed twice with 30uL diH2O for 30s and blocked with 30uL 1% BSA for 30mins. Grids were then incubated with sera/CSF/primary antibody in 30uL 1% BSA for 1h at room temperature and then washed three times with 30uL 1% BSA for 30s. Grids were then incubated with 6 nm immunogold conjugated secondary antibody, including Goat-anti-Human IgG (H&L) and Goat-anti-Mouse IgG (H&L) (Electron Microscopy Sciences, Hatfield, PA) (1:20 dilution in 1% BSA, 30uL) for 1h at room temperature. Afterwards, grids were washed three times with 30uL PBS for 30s and fixed with 30uL 2% glutaraldehyde for 5mins. Finally, grids were washed with 30uL diH20 for three times and stained with 30uL 1% uranyl acid for 1 min. The grids were imaged using a FEI Tecnai T12 Transmission Electron Microscope operated at 120kV.

Enzyme-Linked Immunosorbent Assay (ELISA)

ELISAs were used to determine the titer and binding affinity of antibodies in human CSF and mice sera to different antigens. Maxisorp plates (Thermo Fisher Scientific, Waltham, MA) were coated overnight with 2μg/mL of purified PNMA2 capsids or PNMA2 L270QL325Q protein in assembly buffer at room temperature. PNMA2 fragments were coated in PBS at 4°C. After coating, plates were washed with wash buffer (Thermo Fisher Scientific, Waltham, MA) 5 times and then blocked with 5% Bovine Serum Albumin (BSA; Sigma-Aldrich, St. Louis, MO) in PBS for 2 hours at 37°C. CSF and sera were diluted serially in 1% BSA and incubated with the plates for 2 hours at 37°C. After washing, plates were incubated with anti-mouse IgG or anti-human IgG (1:5000 in 1% BSA; Jackson Laboratory, Bar Harbor, ME) for 1 hour at 37°C. Afterwards, plates were washed and incubated with 3,3',5,5'-Tetramethylbenzidine (TMB) substrate (Thermo Fisher Scientific, Waltham, MA) for 30 mins at 37°C. The enzyme reaction was stopped by adding the stop buffer (Thermo Fisher Scientific, Waltham, MA) and the absorbance was measured at 450nm.

BMDC Culture Differentiation and Flow Cytometry

BMDC cultured cells were stimulated on day 7 by adding either LPS (Invivogen, San Diego, CA) or PNMA proteins to the culture media. Some PNMA protein was pre-incubated with Proteinase K (NEB, Ipswich, MA) for 15 minutes at room temperature according to

manufacturer's recommendations, followed by inactivation at 95 degrees C for 10 minutes. 24 hours later, cells were collected and analyzed by flow cytometry.

To harvest BMDCs for flow cytometric analysis, media was aspirated, and cells were washed with PBS. A cell scraper was used to lift adherent cells, which were then transferred to 5mL Polystyrene Round-Bottom tubes (Falcon) for staining. BMDCs were stained with a cocktail of antibodies for flow cytometry (Flow panel: FC block – TruStain FcX PLUS (anti-mouse CD16/32, Biolegend #156603, San Diego, CA); Viability – PI (Biolegend #421301; MHCII – FITC (Biolegend #107605); CD11c – PE-Cy7 (Biolegend #117317); CD80 – BV421 (Biolegend #104725); CD86 – BV510 (Biolegend #105039); CD83 – BV650 (Biolegend #121515) by centrifuging the cells at 300xg for 5 minutes and resuspending in FACS buffer. Cells were first incubated with FC block (Biolegend, San Diego, CA) at 1:50 for 10 minutes at 4 degrees C. All primary antibodies were then added at a 1:200 dilution and incubated for 20 minutes at 4 degrees C. Excess FACS buffer was added, cells were centrifuged at 300xg for 5 minutes, and resuspended in 200μL FACS buffer plus PI (Biolegend, San Diego, CA) added at 1:100 for flow cytometric analysis.

Flow cytometry was performed on a BD FACSCelesta. At least 20,000 events were collected per sample. Compensation was determined using single-stain controls with the antibodies listed above and the FACSDiva automated compensation system. Flowjo (Treestar, Ashland, OR) was used to generate data. Events were first gated on cells using Forward and Side Scatter, then live cells using propidium iodide-negative cells. Mature DCs were gated as $MHCII^{++}$, $CD11c^{+}$ cells. The mean fluorescence intensity (MFI) of mature DCs was calculated in Flowjo for CD80, CD83, and CD86.

Statistics were generated using a standard two-way ANOVA with Dunnet's multiple comparisons test.

Cytokine Quantification

Cytokines were measured using the ProcartaPlex Mouse Cytokine & Chemokine Convenience Panel 1 26-Plex (Invitrogen, Waltham, MA) on a MAGPIX instrument (Luminex, Austin, TX) according to manufacturer's directions. Briefly, BMDC cell culture supernatants were collected 24 hours post stimulation with the indicated concentration of LPS or PNMA2 protein and centrifuged at 300xg for 5 minutes at 4 degrees C; 50μL of clarified supernatant was used for the assay. Data were analyzed using the ProcartaPlex Analysis App (ThermoFisher, Waltham, MA), and statistical comparisons between assembled capsid versus L/Q mutant were generated using unpaired t test.

Mouse Behavior - Contextual Fear Conditioning

Mice were placed in a fear conditioning chamber (Med Associates Inc, St. Albans, Vermont) with 2% acetic acid. 3 minutes after entering the chamber, the animals were exposed to a 2s electric shock at 0.75mA. The shock was repeated 4 times, with a 60s interval between each trial. Mice were then removed from the chamber 2 minutes after the final shock. Freezing rate during training was measured as follows: Pre-shock freezing was 30s before the 1^{st} shock. Inter-shock interval (ITI) 1-4 were 30s bins from 30^{th} second after each shock. The average and maximum motion of mice during the shock were measured with 5s bin from the beginning of each shock. Memory is tested 24h after training with mice placed in the same conditioning chamber with 2% acetic acid. Freezing was measured during the 3-minute recall test.

RNA-seq Data Analysis

We obtained the processed single-cell expression matrix (counts) from Allen's brain map (https://portal.brain-map.org) representing the human cortex and mouse cortex-hippocampus. We then used Seurat (v3.1.1; https://github.com/satija.lab/seurat https://github.com/satijalab/seurat) within the R environment (v3.6.0) for processing the dataset. We kept the cells with minimum and maximum of 1,000 and 5,000 genes expressed ($\geq$1 count), respectively. Moreover, cells with more than 5% of counts on mitochondrial genes were filtered out. The data normalization was achieved by scaling it with a factor of 10,000, followed by natural-log transformation. Cell type assignment was performed based on the annotations provided by the original publication, albeit we grouped the clusters into broader lineages of excitatory, inhibitory, Oligodendrocyte precursor cells (OPC), Oligodendrocytes and Glial cells (Astrocytes and Microglia). All the given annotations were further confirmed by their respective markers. The expression levels of each gene in a cluster correspond to the average $\log_2$ expression level scaled to the number of unique molecular identification (UMI) values captured in single cells. Finally, the sample replicates for each gene were aggregated per cell type, and their expression was calculated as trimmed means. For the analysis of Human, Chimpanzees and Macaque, we downloaded the human brain transcriptome from 33 major regions representing four adult healthy human individuals, three chimpanzees, and three rhesus macaques (GSE 127898). Trimmed mean of M (TMM) values normalized transcripts per million (TPM) values were imported in R, and variable features were identified when the ratio of variance and mean expression values were greater than one.

QUANTIFICATION AND STATISTICAL ANALYSIS

Data were analyzed using GraphPad Prism. Mann-Whitney test, paired t-test, or two-tailed t-test, one-way ANOVA, and two-way ANOVA were used for the analysis. Not significant (ns) $p>0.05$; *$p<0.05$; **$p<0.01$; ***$p<0.001$; ****$p<0.0001$.

Supplemental figures

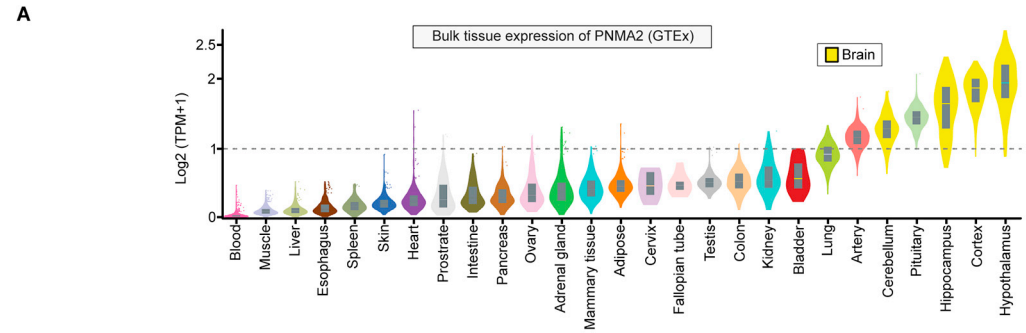

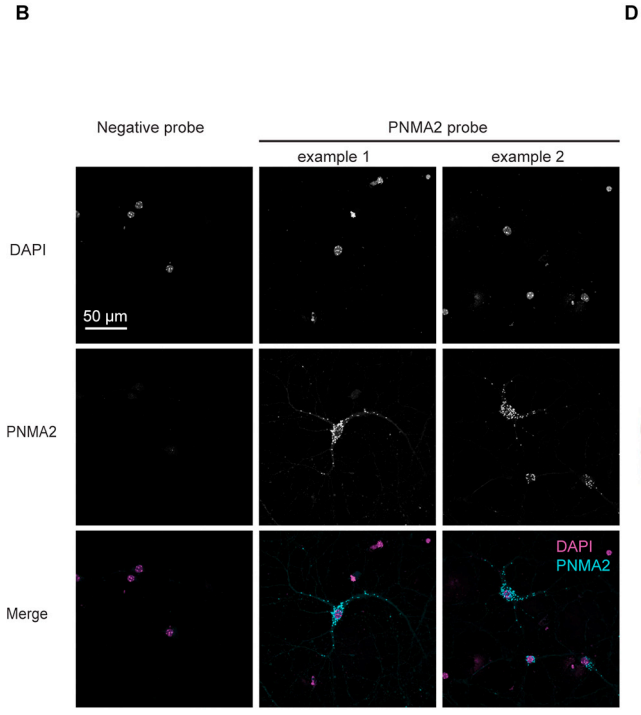

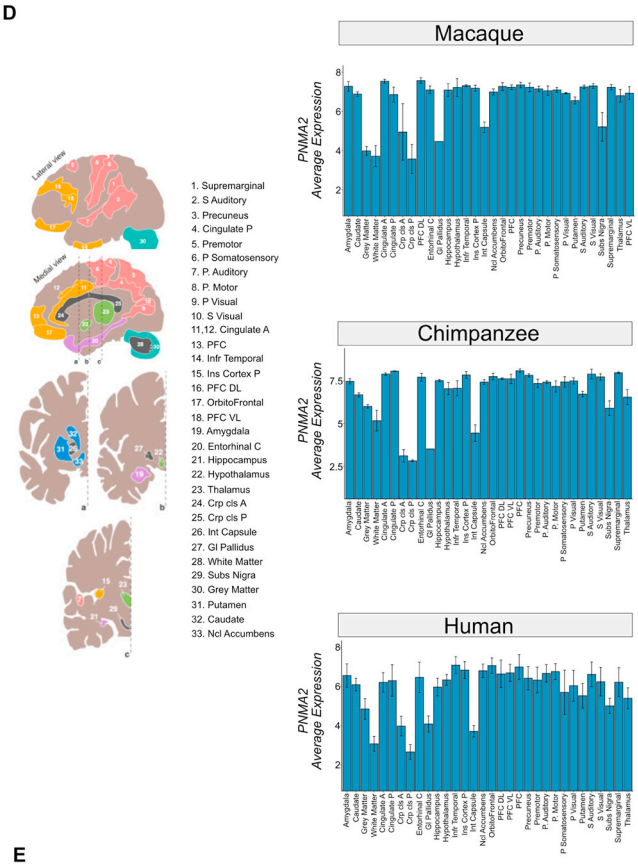

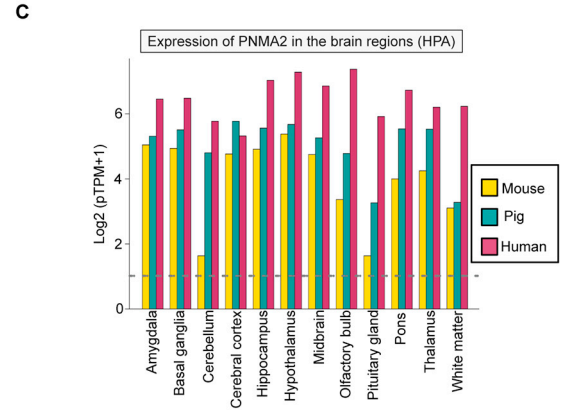

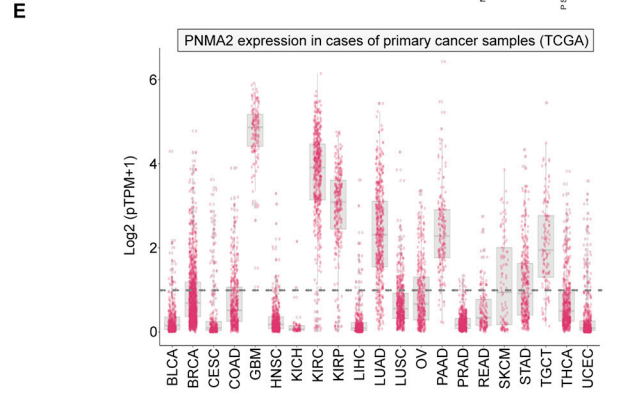

(legend on next page)

Figure S1. PNMA2 is highly expressed in brain and cancer cells, related to Figure 1

(A) Violin plots show the level of bulk RNA expression (log_2 (TPM + 1)) of the *PNMA2* gene from various adult tissues covered and analyzed by the Gtex consortium (https://www.gtexportal.org/home/gene/ENSG00000240694). Multiple tissues from the same organ were aggregated to simplify the visualization.

(B) Representative images of single molecule *in situ* hybridization (RNAscope) for PNMA2 mRNA in cultured mouse hippocampal neurons (DIV15).

(C) Grouped bar plots demonstrate the conservation of *PNMA2* expression in the brain regions of three mammalian species (mouse, pig, and human) shown with the respective color codes. The expression profile of *PNMA2* is shown at log_2 pTPM levels, which is the RNA expression unit normalized to transcripts per million protein coding genes (pTPM), from the human protein atlas platform (HPA).

(D) Combined bar plots show the level of RNA expression of *PNMA2* (log_2 pTPM) from the major structures of 33 brain regions by the analysis of 422 polyA-selected RNA-seq datasets in total. The data represent four adult healthy humans, three chimpanzees, and three rhesus macaques. Error bars show the mean ± standard error of the replicates between individuals.

(E) Jittered boxplots display the gene expression (log_2 pTPM) of *PNMA2* in primary cancer samples of patients from the Cancer Genome Atlas (TCGA) consortium (https://docs.gdc.cancer.gov/Encyclopedia/pages/Annotations_TCGA). All the values of *PNMA2* expression in each cancer samples are denoted as dots in the represented boxplot. Note that testicular cancer (TGCT), pancreatic cancer (PAAD), lung adenocarcinoma (LUAD), kidney renal clear cell (KIRK) and papillary cell carcinoma (KIRP), and grade IV glioblastoma (GBM) display a higher level of *PNMA2* expression compared with the rest of cancer types.

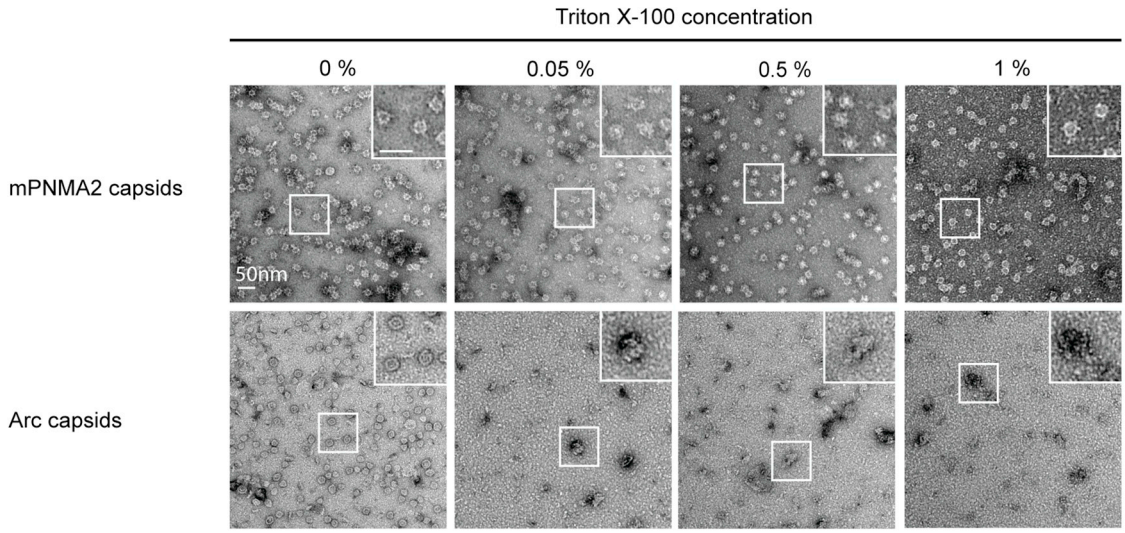

Figure S2. mPNMA2 forms capsids that are resistant to detergent, related to Figure 2

Representative negative-staining EM images of purified mPNMA2 and Arc capsids incubated with different concentrations (0%, 0.05%, 0.5%, 1%) of Triton X-100. Arc capsids are sensitive to detergent, whereas PNMA2 capsids remain intact even after incubation in high detergent levels.

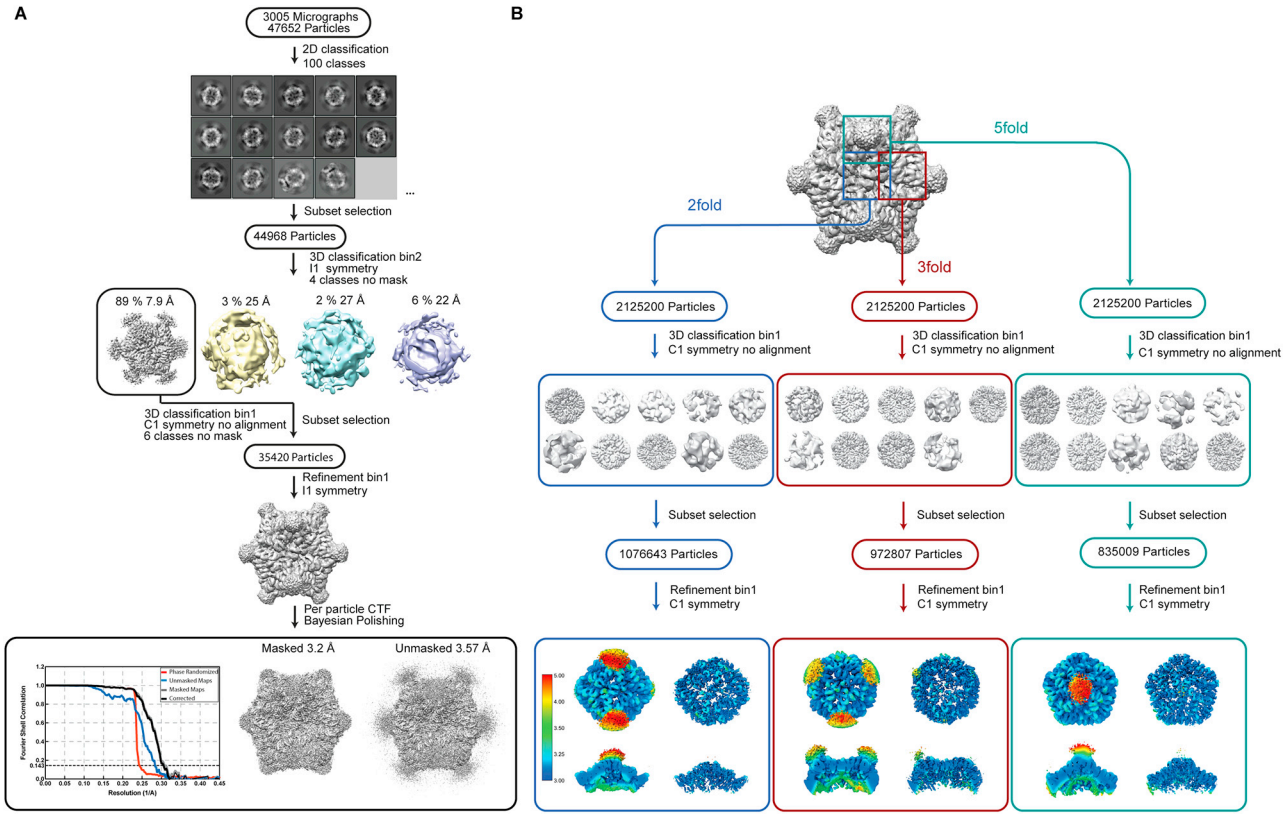

Figure S3. Image processing flowchart for mPNMA2 capsid density map reconstruction, related to Figure 2

(A) Icosahedral mPNMA2 density map reconstruction. Resolution of reconstructions are determined by gold-standard Fourier shell correlation (FSC) at the 0.143 criterion.

(B) Local density map reconstructions. See STAR Methods for details. The unsharpened and sharpened maps of locally refined 5-, 3- and 2-fold symmetric axes are colored from high (blue) to low (red) local resolutions calculated using ResMap. See also Video S3.

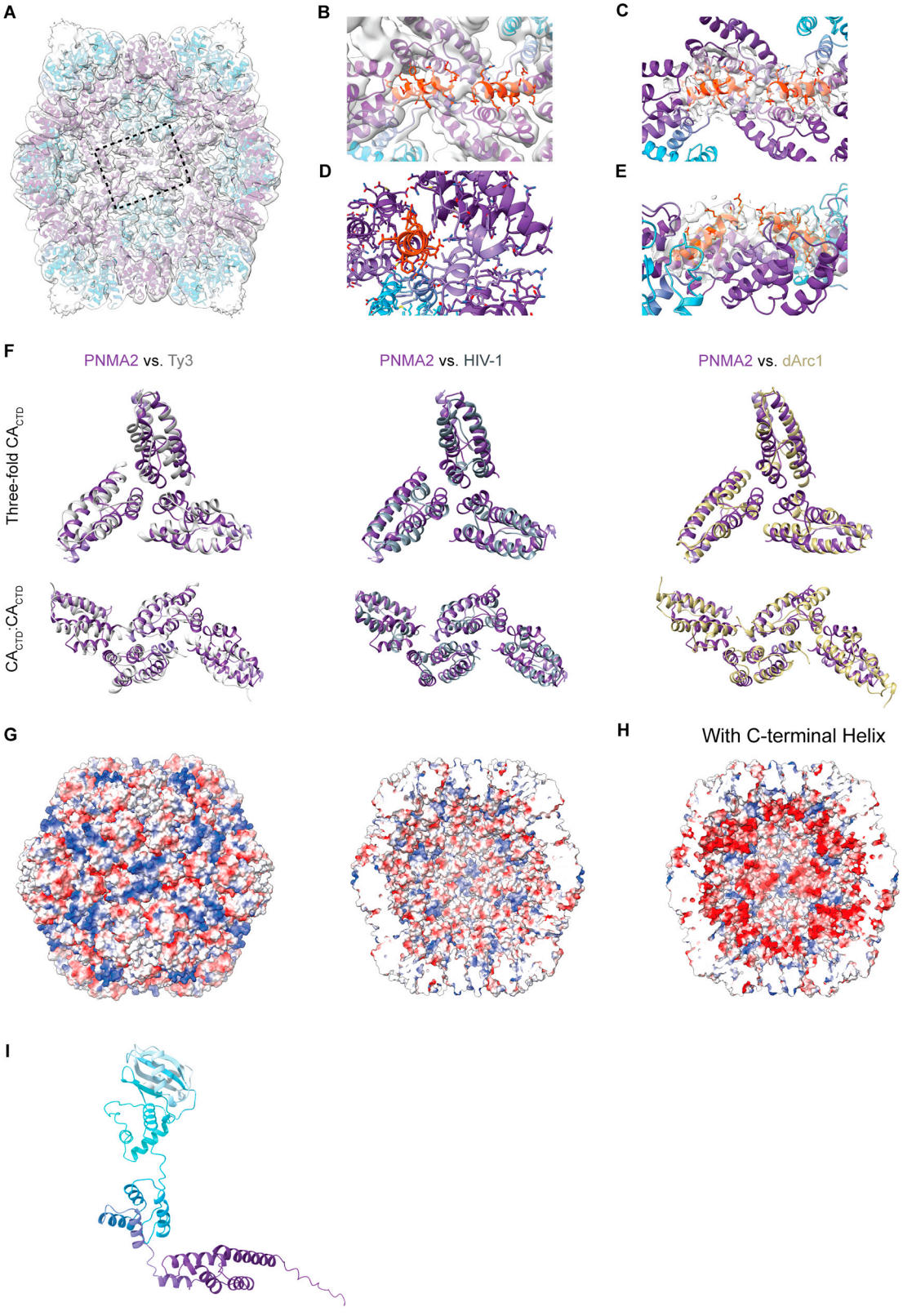

(legend on next page)

Figure S4. Detailed overview of mPNMA2 capsid interfaces and charges, related to Figure 2

(A–E) Different views of the tentative models of the C-terminal CA extension (red). The density is not well resolved in this region, but it is clear that the negatively charged 20-aa region C-terminal of the CA domain extends into the 2-fold CA_{CTD}:CA_{CTD} positively charged interface. This may constitute a potential mechanism for regulation of unspecific nucleic acid binding in larger mPNMA2 capsids.

(F) Alignment of the mPNMA2 capsomer interfaces compared with dArc1, Ty3 and mature HIV capsid interfaces. The arrangement of CA_{CTD} at the 5-, 3-, and 2-fold interfaces in the mPNMA2 capsid is similar to the arrangement at the corresponding positions in Ty3 (light gray), mature HIV-1 (PDB: 5MCX; dark gray) and dArc1 (PDB: 6TAP; yellow). For monomer alignments see Video S2.

(G and H) mPNMA2 capsid exterior and interior surfaces colored by electrostatic potential from −5 (red) to +5 kbT/e (blue). Building in the poorly resolved C-terminal acidic extension makes the inner surface highly negatively charged (H).

(I) Alphafold2 predicted model of mPNMA2. CA domain in purple and spike domain, which is unresolved in the cryo-EM capsid structure shown in cyan.

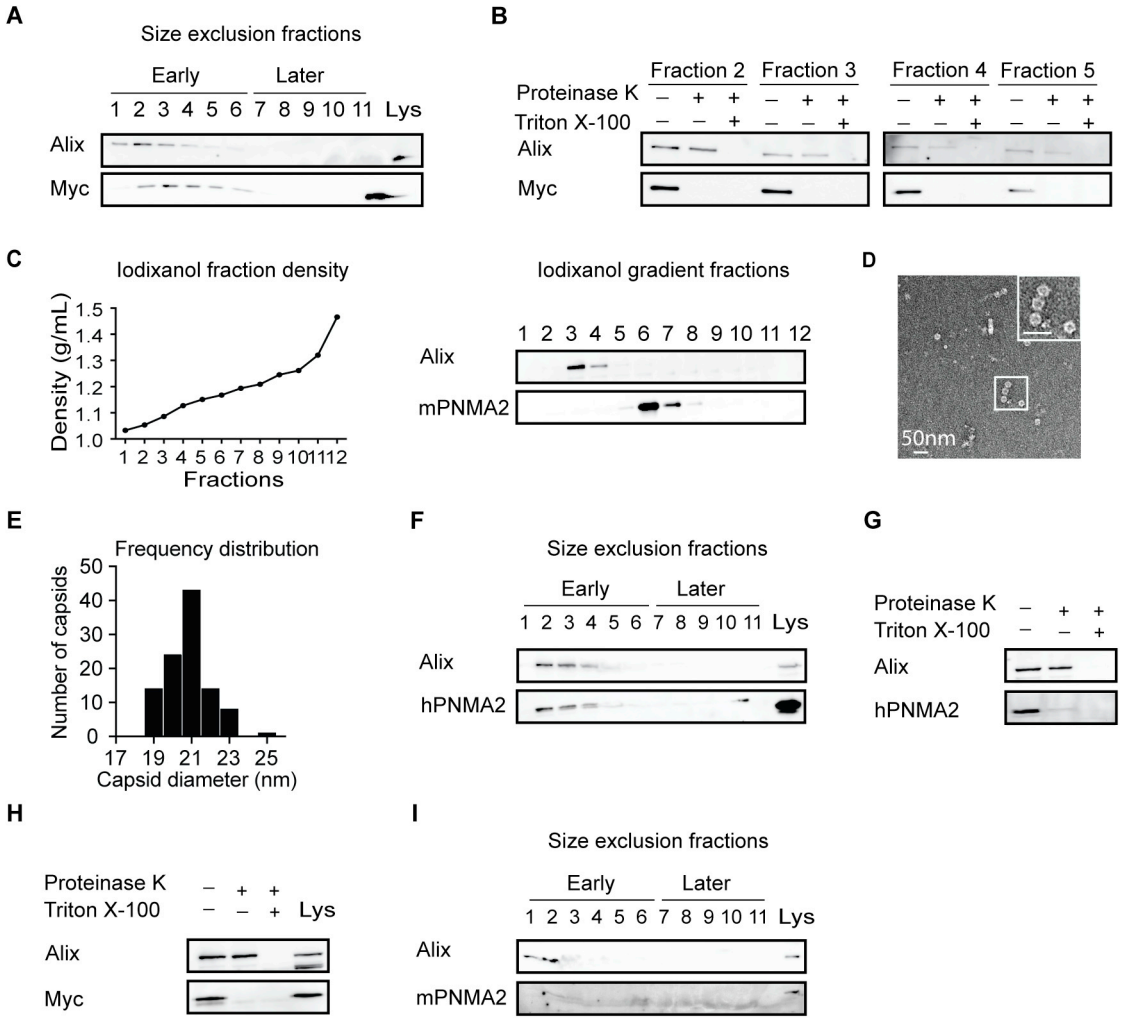

Figure S5. PNMA2 is released as non-enveloped capsids in various cell lines, related to Figure 3

(A) Media was collected from myc-mPNMA2 transfected in HEK293T cells and fractionated using size exclusion chromatography (SEC). Fractions were run on a gel and blotted for myc and ALIX. mPNMA2 protein is released in early fractions that contain EV proteins.

Abbreviation is as follows: Lys, cell lysate.

(B) The early SEC fractions (2–5) from myc-mPNMA2 transfected HEK293T culture media were blotted for myc and ALIX. One set of fractions were incubated with proteinase K (7 μg/mL) with or without detergent present (1% Triton X-100) for 10 min. Representative western blots show that mPNMA2 protein is sensitive to proteinase K degradation without detergent present.

(C) The pooled early SEC fractions (1–6) from myc-mPNMA2 transfected HEK293T culture media were further fractionated using ultracentrifugation. An iodixanol gradient was used to separate proteins by density and size. mPNMA2 protein was enriched in fraction 6, while ALIX was enriched in fractions 3 and 4.

(D) A representative negative-staining EM image of non-enveloped mPNMA2 capsids isolated from the iodixanol gradient fraction 6 in (C).

(E) The quantification of capsid diameters in iodixanol gradient fraction 6 imaged by negative-staining EM. These capsids show similar morphology and size to purified mPNMA2 capsids from *E. coli*.

(F) Media was collected from NCI-H378 cell culture and fractionated using SEC. Fractions were run on a gel and blotted for hPNMA2 and ALIX. hPNMA2 protein is released in early fractions that contain EV proteins.

(G) The early SEC fractions (1–3) from NCI-H378 cell culture media were pooled and blotted for hPNMA2 and ALIX. Fractions were incubated with proteinase K (7 μg/mL) with or without 1% Triton X-100 for 10 min. Representative western blots show that hPNMA2 protein is sensitive to proteinase K degradation without detergent present.

(H) Media was collected from myc-mPNMA2 overexpressed in NTERA-2 cell culture and fractionated using SEC. The early fractions (1–3) were pooled and blotted for myc and ALIX. Fractions were incubated with proteinase K (7 μg/mL) with or without 1% Triton X-100 for 10 min. Representative western blots show that mPNMA2 protein is sensitive to proteinase K degradation without detergent present.

(I) Media was collected from mPNMA2 overexpressed in MC-38 cultured cells and fractionated using SEC. Fractions were run on a gel and blotted for mPNMA2 and ALIX. mPNMA2 protein was not released into culture media.

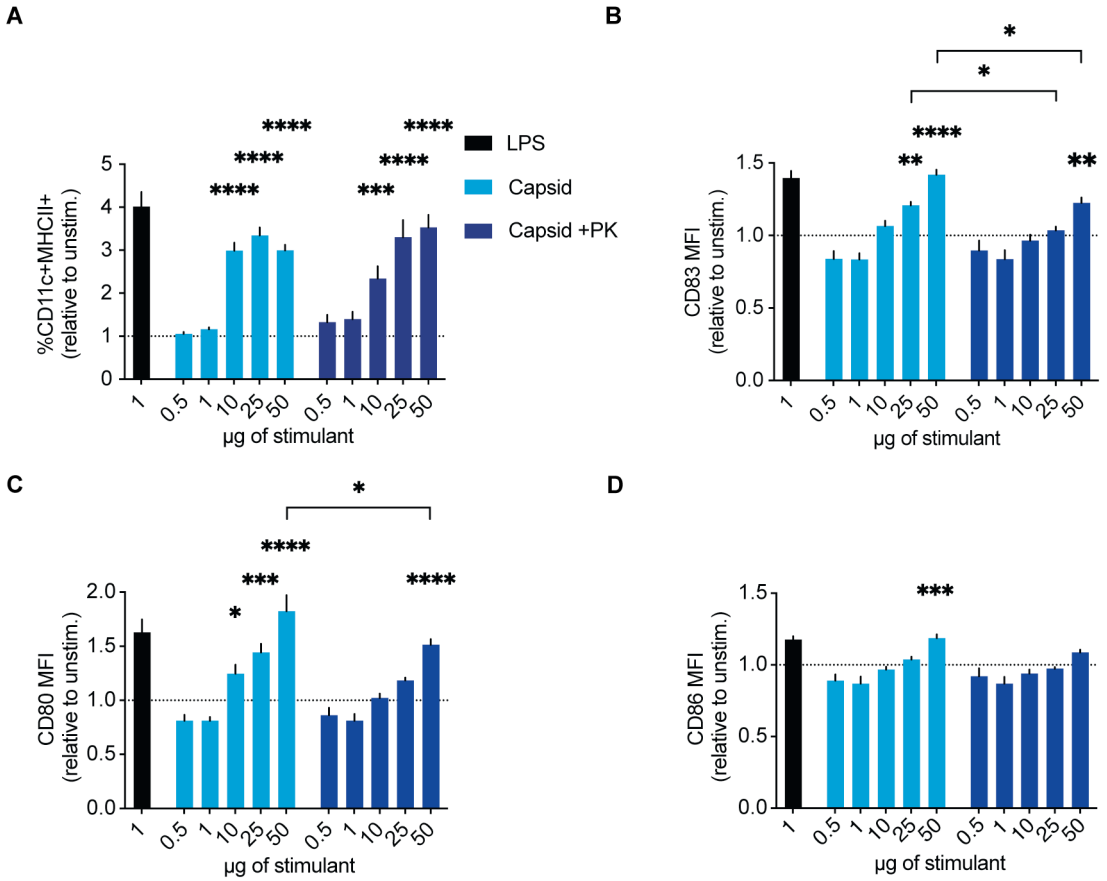

Figure S6. mPNMA2 capsids activate bone marrow-derived dendritic cells, related to Figure 6

(A) Murine bone marrow cells were isolated and cultured with 20 ng/mL GM-CSF for 7 days to generate bone-marrow-derived dendritic cells (BMDCs), which were then activated with varying concentrations of the indicated stimuli for 24 h prior to flow cytometric analysis. Data show quantification of matured ($CD11c^{+}MHCII^{++}$) BMDC following stimulation, graphed as fold increase relative to unstimulated BMDC of the same experiment. n = 4 independent experiments. (B–D) Mean fluorescence intensity of CD83 (B), CD80 (C), and CD86 (D) within the matured BMDC population graphed as fold increase relative to unstimulated BMDC of each independent experiment. mPNMA2 capsids induced more robust increases in CD83, CD80, and CD86 than proteinase-K-treated capsids. Data represent mean ± SEM of n = 4 biological replicates. Statistics for comparisons across treatment groups were determined using a two-way ANOVA with Šídák's multiple comparisons test, $^{*}p < 0.05$. To determine whether cell surface markers were significantly upregulated compared with baseline, two-way ANOVA was performed with Dunnett's multiple comparisons test using unstimulated values as a control, $^{*}p < 0.05$, $^{**}p < 0.01$, $^{***}p < 0.001$, $^{****}p < 0.0001$.

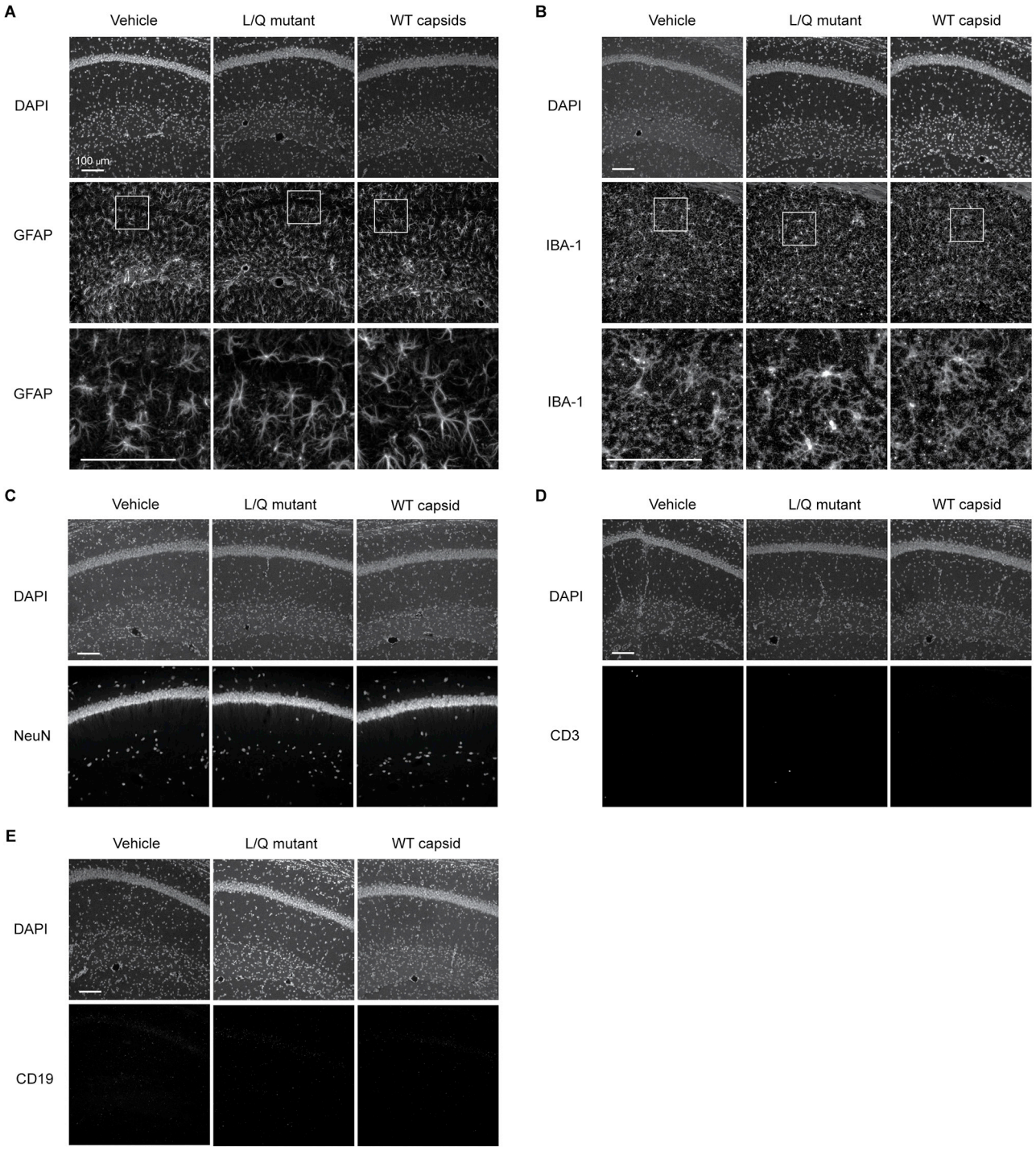

Figure S7. PNMA2-capsid-injected mice do not show gross brain pathology, related to Figure 7

Immunohistochemistry of mouse hippocampus sections from vehicle, mPNMA2 L/Q mutant and WT capsids injected mice, using antibodies to: (A) astrocytes (GFAP), (B) microglia (IBA-1), (C) neurons (NeuN), (D) T cells (CD3), (E) B cells (CD19). No overt brain pathology observed in mPNMA2 capsid-injected mice 6 months after immunization. Scale bars, 100 μm.